

# **Dimensionality reduction to maximize prediction generalization capability**

Takuya Isomura<sup>1\*</sup>, Taro Toyoizumi<sup>1,2\*</sup>

<sup>1</sup> Laboratory for Neural Computation and Adaptation, RIKEN Center for Brain Science, Wako, Saitama 351-0198, Japan

<sup>2</sup> Department of Mathematical Informatics, Graduate School of Information Science and Technology, The University of Tokyo, Bunkyo-ku, Tokyo 113-8656, Japan

\* Corresponding author email: [takuya.isomura@riken.jp](mailto:takuya.isomura@riken.jp), [taro.toyoizumi@riken.jp](mailto:taro.toyoizumi@riken.jp)

Keywords: predictive coding, dimensionality reduction, noise reduction, system identification

## Abstract

This work develops an analytically solvable unsupervised learning scheme that extracts the most informative components for predicting future inputs, termed predictive principal component analysis (PredPCA). Our scheme can effectively remove unpredictable observation noise and globally minimize the test prediction error. Mathematical analyses demonstrate that, with sufficiently high-dimensional observations that are generated by a linear or nonlinear system, PredPCA can identify the optimal hidden state representation, true system parameters, and true hidden state dimensionality, with a global convergence guarantee. We demonstrate the performance of PredPCA by using sequential visual inputs comprising hand-digits, rotating 3D objects, and natural scenes. It reliably and accurately estimates distinct hidden states and predicts future outcomes of previously unseen test input data, even in the presence of considerable observation noise. The simple model structure and low computational cost of PredPCA make it highly desirable as a learning scheme for biological neural networks and neuromorphic chips.

Prediction is essential for both biological organisms [1,2] and machine learning [3,4]. In particular, they need to predict the dynamics of newly encountered sensory input data (i.e., test data) based on and only on knowledge learned from a limited number of past experiences (i.e., training data). Generalization error is a standard measure of the generalization capability of predicting the future consequences of previously unseen input data, which is defined as the difference between the training and test prediction errors. It is thus crucial for organisms and

machines to find a prediction strategy with a small generalization error, as otherwise their predictions will fail owing to overfitting to the training data.

Despite the importance of generalizing prediction, current mainstream machine learning approaches have some limitations. They can be categorized into three major groups, and their limitations are summarized as follows: (1) The most basic prediction strategy is to learn a direct mapping from past to future inputs in the form of autoregressive (AR) model (**Fig. 1a**). Although AR models are simple to construct and guarantee global convergence, their predictions contain a large generalization error because the mapping from the observations to the prediction is often redundant, leading to severe overfitting when the number of training samples is limited [5,6]. Thus, to make accurate predictions, low-dimensional (i.e., concise) representations should be extracted from high-dimensional (i.e., redundant) sensory data. (2) A dimensionality reduction technique can be used to obtain a concise representation [7]; however, this is often achieved separately from the prediction step—e.g., by first applying an autoencoder to reduce the dimensionality [8,9] and then employing a long short-term memory to predict the sequence [10] (**Fig. 1b**). The first autoencoding step—which provides a low-dimensional representation that minimizes the loss for reconstructing the current input—is the most basic dimensionality reduction strategy. One problem of this approach is that autoencoders may preferentially extract observation noise that is useless for prediction, owing to its extra variance. (3) A major approach to time-series prediction is to construct a state-space model (SSM). SSMs, which include the Kalman filter [11] and its nonlinear variants [4,12,13], simultaneously perform dimensionality reduction and prediction (**Fig. 1c**). From

this model-based perspective, the best prediction is achieved when an SSM employs the states and parameters that match the true system properties. However, the problem becomes difficult when both the hidden states and system parameters are unknown. In particular, their predictions become inaccurate owing to nonlinear interactions between the uncertainties in hidden states and parameters, as they can create spurious solutions. Furthermore, the dimensionality of hidden states, which is essential for prediction accuracy, is hard to optimize. Conventional model selection approaches using some information criterion [14–16] or cross-validation [17] would fail to identify the optimal dimensionality when the state or parameter estimation converges to a suboptimal solution. In short, all three approaches have essential drawbacks that interfere with the generalization of accurate predictions. To overcome these limitations, we establish a method that can solve this simultaneous optimization problem of hidden states, system parameters, and dimensionality with a global convergence guarantee.

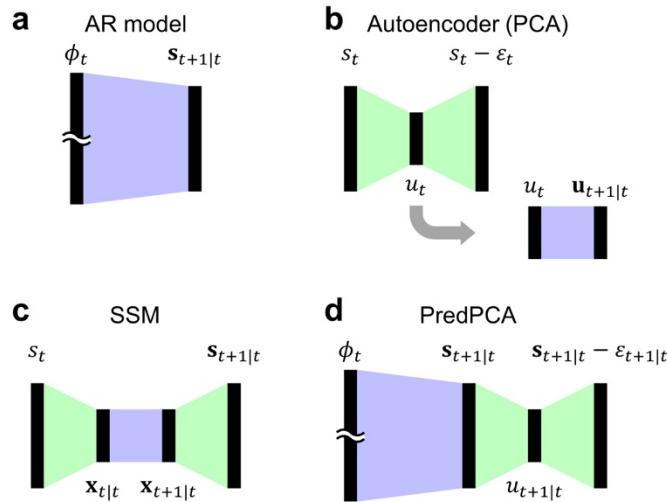


**Figure 1.** Four different prediction-model structures. A black bar denotes a layer of a neural

network, while blue and green trapezoids denote synaptic weight matrices for prediction and dimensionality reduction, respectively. **(a)** Naïve AR models directly compute the maximum likelihood estimator of the next input  $\mathbf{s}_{t+1|t}$  based on the bases  $\phi_t \equiv (s_t^T, s_{t-1}^T, s_{t-2}^T, \dots)^T$  that summarize current and past observations. **(b)** Two-step prediction models first extract a concise representation  $u_t$  using an autoencoder (PCA) by minimizing the loss  $\varepsilon_t$ , and then predict the next representation  $\mathbf{u}_{t+1|t}$  using a recurrent neural network. **(c)** SSMs update the hidden state estimator  $\mathbf{x}_{t|t}$  based on the previous state and current input and predict the next state  $\mathbf{x}_{t+1|t}$  and input  $\mathbf{s}_{t+1|t}$ . **(d)** PredPCA first computes the maximum likelihood estimator  $\mathbf{s}_{t+1|t}$  and then extracts a concise representation  $u_{t+1|t}$ , by minimizing the prediction error  $\varepsilon_{t+1|t}$ . This scheme can filter out the causes of the generalization error.

Here, we develop a novel learning scheme for extracting features that are essential for prediction, termed *predictive principal component analysis* (PredPCA). It is formally derived from the minimization of the squared prediction error and can extract low-dimensional predictive features from high-dimensional sensory inputs, even in the presence of observation noise that is much larger than the signals themselves. This robustness is because PredPCA conducts *post-hoc dimensionality reduction* to extract a concise representation of the predicted input, unlike autoencoders or SSMs (**Fig. 1d**). This allows PredPCA to find hidden states (c.f., blind source separation [18–20]) and perform long-term prediction reliably and accurately. In particular, system parameter identification [21,22] using PredPCA contrasts with conventional methods. It is

guaranteed to identify the true system parameters in the large sample-size limit—even for nonlinear generative processes, when the mappings from hidden states to sensory inputs are sufficiently high-dimensional. In addition, based on Akaike’s statistics [14,23], we analytically derive a mathematical formula that estimates the test prediction error of PredPCA. It shows that the generalization error is proportional to an entropy due to the sampling fluctuation [23]. The minimization of this formula can optimize unknown free parameters, including the rank of system dimensions and order of past observations used for prediction, and can provide the global minimum of the test prediction error. We mathematically and numerically demonstrate that filtering out unpredictable noise by using PredPCA is essential to maximize the prediction generalization capability.

## RESULTS

### Predictive principal components analysis (PredPCA)

In this work, we assume that hidden states  $x_t$  generate higher-dimensional sensory inputs  $s_t$  as follows:

$$s_t = g(x_t) + \omega_t, \quad (1)$$

and the dynamics of hidden states are described by

$$x_{t+1} = f(x_t, x_{t-1}, x_{t-2}, \dots) + z_t, \quad (2)$$

where  $z_t$  and  $\omega_t$  are mutually independent white Gaussian noises, with zero means and covariances  $\Sigma_z$  and  $\Sigma_\omega$  (**Fig. 2a**, left, and Methods A). Process noise  $z_t$  adds stochasticity into the hidden state dynamics, while observation noise  $\omega_t$  represents any unpredictable fluctuations that we wish to remove. Although this paper focuses on white Gaussian noise for simplicity, PredPCA's outcomes would also be accurate with colored or non-Gaussian noise, as long as the auto-correlation time constant of  $\omega_t$  is smaller than that of  $x_t$ . **Table 1** presents the glossary of expressions.

PredPCA aims to extract the components containing the most information for predicting the next input  $s_{t+1}$  based on current and past observations  $s_t, s_{t-1}, s_{t-2}, \dots$ . With this in mind, we consider a linear neural network whose output is given by

$$u_{t+1|t} = V\phi_t, \quad (3)$$

where  $u_{t+1|t}$  is an  $N_u$ -dimensional vector of encoders,  $V$  is a (horizontally long)  $N_u \times N_\phi$  encoding synaptic weight matrix, and  $\phi_t \equiv (s_t^T, s_{t-1}^T, s_{t-2}^T, \dots)^T$  is an  $N_\phi$ -dimensional vector of linear basis functions that summarize current and past observations. Unlike standard principal component analysis (PCA) [24–27] and autoencoders [8,9], which minimize the reconstruction error in the current input, PredPCA minimizes the prediction error  $\varepsilon_{t+1|t} \equiv s_{t+1} - W^T u_{t+1|t}$ , defined as the difference between the actual next input at  $t+1$  and the prediction based on inputs up to  $t$ . Here,  $W^T$  is an  $N_s \times N_u$  decoding synaptic weight matrix used for predicting the next input  $s_{t+1}$  based on the concise encoders  $u_{t+1|t}$  (where we introduced  $W^T$  rather than  $W$  for a notational reason that will become clear below). PredPCA's cost function  $L$  is given by the

expectation of the squared prediction error over the training period  $T$ :

$$L \equiv \frac{1}{2} \left\langle |\varepsilon_{t+1|t}|^2 \right\rangle_q. \quad (4)$$

Here,  $\langle \cdot \rangle_q \equiv \frac{1}{T} \sum_{t=1}^T \cdot$  indicates the expectation over the empirical distribution  $q$ . By minimizing this cost function with respect to  $V$ , we obtain the optimal encoding weights as  $V = W\mathbf{Q}$ , where  $\mathbf{Q} \equiv \langle s_{t+1} \phi_t^T \rangle_q \langle \phi_t \phi_t^T \rangle_q^{-1}$  (Methods B). Thus,  $u_{t+1|t} = W\mathbf{s}_{t+1|t}$  holds, where  $\mathbf{s}_{t+1|t} = \mathbf{Q}\phi_t$  is the maximum likelihood estimator of  $s_{t+1}$ . The synaptic weight matrix  $W$  is updated by gradient descent based on  $L$ . After some additional transformations (Methods B), we obtain

$$\dot{W} \propto -\frac{\partial L}{\partial W} = \left\langle u_{t+1|t} (s_{t+1} - W^T u_{t+1|t})^T \right\rangle_q. \quad (5)$$

The fixed point of Equation (5) yields the transpose of optimal decoding weights that minimize  $L$ .

The solution implies that the encoders  $u_{t+1|t}$  achieve the optimal representation for prediction.

Equation (5) is equivalent to the subspace rule of PCA [26], except that  $u_{t+1|t}$  encodes the future state at time  $t+1$  instead of the state at time  $t$  (i.e., the standard PCA uses  $u_{t|t}$ ). This means that PredPCA, which is defined by the prediction error minimization, can be decomposed into two steps: computing the maximum likelihood estimator of  $s_{t+1}$ ,  $\mathbf{s}_{t+1|t}$ , followed by a post-hoc PCA of  $\mathbf{s}_{t+1|t}$  using the eigenvalue decomposition (**Fig. 1d**). Owing to the global convergence property of the subspace rule for PCA [28], the global convergence of Equation (5) is also guaranteed; thus, PredPCA is a convex optimization. Crucially, however, only PredPCA (but not the standard PCA) can effectively filter out unpredictable observation noise, as we demonstrate numerically below and mathematically in Methods C. Note that although this paper focuses on the prediction of



subsequent inputs (i.e., autoregression), it is straightforward to apply PredPCA to minimize the generalization error for a class of regression tasks (which is simply formulated by supposing that the hidden states  $x_t$  generate both observations  $s_t$  and a high-dimensional target signal  $y_t$  and by replacing the prediction error  $\varepsilon_{t+1|t}$  with  $\varepsilon_t \equiv y_t - W^T V \phi_t$ ).

After extracting the hidden states by using PredPCA, we employ independent component analysis (ICA) [29–31], which can separate the extracted states into independent components as long as the true hidden states of the external world are actually mutually independent. For example, when the network observes a sequence of MNIST handwritten digits [32], PredPCA followed by ICA generates 10-dimensional independent encoders  $\tilde{u}_{t+1|t}$ , each element of which encodes one of the 10 possible digits (**Fig. 2a**, right).

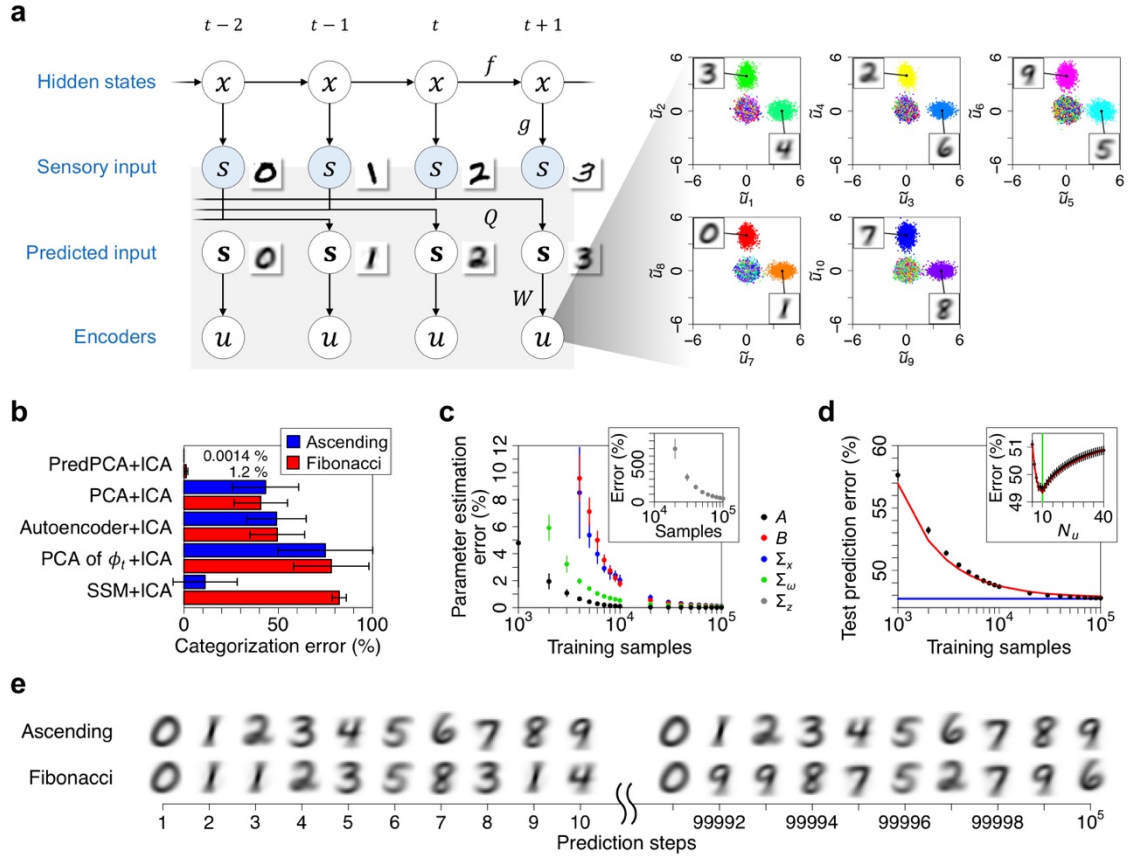


**Figure 2.** PredPCA of handwritten digit sequences. **(a)** Left: System comprising a generative process (top) and a neural network that follows PredPCA (bottom, shaded). The network is trained with an image sequence  $s_t$  of handwritten digits generated from the dynamics of 10-dimensional hidden states  $x_t$ , each element of which expresses one of the 10 digits. Right: 10-dimensional independent encoders  $\tilde{u}_t$  obtained using PredPCA and ICA.  $2 \times 10^4$  test samples that are color-coded by their digit are plotted. **(b)** Comparison with related methods in terms of the mean categorization error (i.e., false discovery rate). The digits are introduced in ascending order (blue) and Fibonacci sequence (red) with some randomness. The error bars indicate the standard deviation. **(c)** Parameter estimation error measured by the squared Frobenius norm ratio, where the difference between the true parameter matrix  $\theta$  and its estimator  $\hat{\theta}$  is divided by the norm of  $\theta$ ,  $error = \|\hat{\theta} - \theta\|_F^2 / \|\theta\|_F^2$ . PredPCA assumes here that the ascending-order handwritten digit

sequence is generated from a linear system comprising  $s_t = Ax_t + \omega_t$  and  $x_{t+1} = Bx_t + z_t$  ( $A$ , black,  $B$ , red). The covariance matrices  $\Sigma_x$  (blue),  $\Sigma_\omega$  (green), and  $\Sigma_z$  (gray, inset) are associated with  $x_t, \omega_t, z_t$ , respectively. **(d)** Test prediction error in the ascending-order sequence, measured by the normalized mean squared error over test samples,  $error = \left\langle |s_{t+1} - W^T u_{t+1|t}|^2 \right\rangle / \langle |s_{t+1}|^2 \rangle$ . The red line (in the main and inset panels) represents a theoretical prediction obtained using Equation (7). The blue line denotes the lower bound of the error, calculated via supervised learning. The inset panel depicts the dependence of the test prediction error on the encoding dimensionality  $N_u$  (when  $T = 6000$ ), where  $N_u = 10$  (green line) is optimal. (b)(c)(d) are obtained with 10 different realizations of digit sequences. Note that the error bars in (d) are hidden by the circles. **(e)** Long-term prediction using PredPCA and ICA. A winner-takes-all operation is applied to make greedy predictions of the digit sequences. After receiving the first 40 digits, unless those initial digit images are outliers, the network can predict the next  $10^5$  digits (and more) without any categorization error. See Method G for further details.

## Key analytical discoveries

We conducted comprehensive mathematical analyses to rigorously demonstrate the performance and statistical properties of PredPCA. In particular, we demonstrated the following two key properties: (1) It is mathematically guaranteed that PredPCA can identify the *optimal* (explained below) hidden state representation and parameter estimators—up to a linear transformation that does not affect prediction accuracy—for general linear systems and,

asymptotically, even for nonlinear systems (Methods E, F). While using a linear neural network for the encoding, the asymptotic linearization theorem [33] ensures that PredPCA will extract true hidden states when the mappings from hidden states to sensory inputs are sufficiently high-dimensional. Briefly, this is because projecting the high-dimensional input onto the directions of its major eigenvectors effectively magnifies the linearly transformed components of the hidden states included in the input, while filtering out the nonlinear components (see Methods E for its mathematical statement and the conditions for application; see [33] for the mathematical proof). Owing to this linearization property,  $u_{t+1|t}$  asymptotically converges to a linear transformation of the maximum likelihood estimator of hidden states  $x_{t+1}$ ,  $\langle x_{t+1} \phi_t^T \rangle_q \langle \phi_t \phi_t^T \rangle_q^{-1} \phi_t$ . Hence, PredPCA provides the optimal hidden state representation for prediction. Furthermore, the analytical expressions of the system parameter estimators are derived as functions of the obtained hidden state estimator, with a convergence guarantee to the true parameter values in the large sample-size limit. These parameter estimators are calculated by a simple iteration-free computation summarized in **Table 2** and Method F. This result is surprising because the reliable identification of the optimal hidden states and the true parameters were previously only described within the framework of supervised learning, whereas PredPCA can provide them by unsupervised learning without relying on the true hidden states  $x_t$ .

(2) PredPCA can maximize the prediction generalization capability by minimizing the test prediction error

$$L_{test} \equiv \frac{1}{2} \left\langle |\varepsilon_{t+1|t}|^2 \right\rangle. \quad (6)$$

Here,  $\langle \cdot \rangle \equiv \int \cdot p(\phi_t, s_{t+1}) d\phi_t ds_{t+1}$  indicates the expectation over the true distribution

$p(\phi_t, s_{t+1})$  (note the difference from Equation (4)). In practice, however, the true distribution is unknown for a learner. Thus, one needs to estimate Equation (6) based on and only on parameters estimated using training data. In the framework of the maximum likelihood estimation or squared error minimization, the expectation of the test error is expressed as an Akaike information criterion (AIC) [14] or network information criterion (NIC) [15], respectively. Similar to the derivation of AIC and NIC, we explicitly compute the expectation of Equation (6), with the optimized synaptic weights, as

$$\underbrace{\mathcal{L}}_{\text{test error expectation}} \equiv E_{\{q\}}[L_{\text{test}}] = \underbrace{\frac{1}{2}(\text{tr}[\mathbf{\Sigma}_s] - \text{tr}[\mathbf{P}_s^T \mathbf{\Sigma}_s \mathbf{P}_s])}_{\text{training error}} + \underbrace{\frac{N_\phi}{2T} \text{tr}[\mathbf{P}_s^T (\mathbf{\Sigma}_s - \mathbf{\Sigma}_s) \mathbf{P}_s]}_{\text{generalization error}} + \mathcal{O}\left(T^{-\frac{3}{2}}\right). \quad (7)$$

See Methods D for the derivation. Here,  $T$  is the number of training samples,  $\mathbf{P}_s$  is the first-to- $N_u$ -th major eigenvectors of the predicted input covariance  $\mathbf{\Sigma}_s \equiv \langle \mathbf{s}_{t+1|t} \mathbf{s}_{t+1|t}^T \rangle_q$  (where  $W^T W = \mathbf{P}_s \mathbf{P}_s^T$  holds at the fixed point of Equation (5)), and  $\mathbf{\Sigma}_s \equiv \langle s_t s_t^T \rangle_q$  is the actual input covariance. The expectation  $E_{\{q\}}[\cdot]$  is taken over different empirical distributions  $q$ , each of which comprises  $T$  training samples and is used to optimize synaptic weights. The expectation of the test prediction error  $\mathcal{L}$  is characterized by two free parameters: the rank of encoding dimensions ( $N_u$ ) and the order of past observations used for the maximum likelihood estimation ( $N_\phi$ ).

Optimizations of  $N_u$  and  $N_\phi$ , with the synaptic weight update by Equation (5), provide the global minimum of  $\mathcal{L}$ . The optimal encoding dimensionality is guaranteed to converge to the true hidden basis dimensionality for a large but finite  $T$  (Methods D). The second term of  $\mathcal{L}$ , referred to as the

generalization error, is associated with an entropy due to the sampling fluctuation [23]. This term indicates that only the prediction error projected to the major eigenspace causes the generalization error, which highlights the importance of dimensionality reduction to reduce the test prediction error. In short, naïvely minimizing the training error by using a large encoding dimensionality, such as in AR models, leads to overfitting; in contrast, minimizing  $\mathcal{L}$  provides the best encoding dimensionality and order of past observations to generalize the prediction.

For further details, please see the Methods and Supplementary Materials. In what follows, we demonstrate the performance of PredPCA using sequential visual inputs comprising handwritten digits, rotating 3D objects, and natural scenes.

### **PredPCA provides optimal representation and parameters for prediction**

In the first experiment (**Fig. 2**), we trained a neural network with MNIST handwritten digit images [32] in ascending order and in the Fibonacci sequence, but with some additional stochasticity such that a digit was replaced by a random one and a monochrome inversion occurred with a small probability at each step. In both cases, PredPCA successfully extracted 10-dimensional features underlying the image sequences as they were relevant to predicting the sequences. The following ICA [31] separated the extracted components into independent hidden states. Each encoder neuron selectively responded to one of the 10 digits without being taught their labels, as we can see for the encoders trained with the ascending sequence in **Fig. 2a** (right).

Regardless of the sequence types (ascending order and Fibonacci sequence), PredPCA and ICA precisely separated the digits into 10 clusters in 10 dimensions with an average categorization error of less than 2% (scored by false discovery rate; **Fig. 2b**). During this process, PredPCA ignored any within-class differences in the digit images that do not predict the next image. Hence, PredPCA’s policy of dimensionality reduction to minimize the prediction error distinguishes it from standard PCA [24–27] and autoencoders [8,9]—because PCA and autoencoders minimize the reconstruction error for the current input  $s_t$  and thus preferentially extract the within-class differences in the digit images due to their extra variances. Even when the standard PCA was applied to the past-to-current input sequence (i.e.,  $\phi_t$ ), it failed to separate the digits because the hidden representation of  $\phi_t$  included more than 10-dimensional state space and thus the first 10 major components of  $\phi_t$  did not match the true hidden states  $x_t$ . The performance of the SSM based on the Kalman filter with 10-dimensional state space was also poor because its larger parameter estimation errors led it to a spurious solution (i.e., local minimum).

In addition to accurate source separation, PredPCA could provide the true system parameters (**Fig. 2c**). These parameter estimators were computed simply by following the definitions in **Table 2**. The differences between the parameter estimators obtained by PredPCA and those obtained by supervised learning converged to zero as the number of training samples increased, as predicted by our theory (Methods F). It is important to note, for the comparison between PredPCA and SSMs, that the estimator of the process noise covariance  $\Sigma_z$  was much less accurate than those of the other parameters, as  $\Sigma_z$  is smaller than  $\Sigma_x$  in magnitude. This inaccuracy is common to both

PredPCA and the SSMs, but it more drastically reduces the SSMs' prediction accuracy as it explicitly uses  $\Sigma_z$  for state prediction, leading to the ensuing inaccuracy of the system identification. By contrast, PredPCA's prediction accuracy is independent of the estimation error in  $\Sigma_z$  as it is not used for the prediction.

The above outcomes allowed PredPCA to predict subsequent digits reliably and accurately (**Fig. 2d**). Here, we see that although PredPCA did not observe the hidden states directly, its test prediction error globally converged, with increasing training samples, to the lower bound of the test prediction error computed via supervised learning that explicitly used the true hidden states for training. This is as theoretically predicted by Equation (7). Moreover, Equation (7) successfully identified the optimal encoding dimensionality that minimized the test prediction error as  $N_u = 10$ , which also matched the true hidden state dimensionality (**Fig. 2d**, inset panel). In particular, the long-term prediction of subsequent digits highlights the significance of PredPCA's categorization and system identification accuracy, as it could recursively predict the subsequent digits without categorization errors for more than  $10^5$  steps (**Fig. 2e**).

### **PredPCA filters out observation noise and minimizes test prediction error**

As shown analytically in Equation (7), filtering out the observation noise by reducing the encoding dimensionality is essential for reducing the generalization error. In **Fig. 3**, the noise reduction and prediction capabilities of PredPCA were examined using natural movies. We trained



a neural network by using images of 3D objects rotating clockwise [34] as the input (**Fig. 3a**, furthest left). In short, the task was to predict the opposite side of test object images (200 objects) by observing only a half side of the images, based on the transition (i.e., rotational) mapping learned from different training object images (up to 800 objects). PredPCA extracted components that were the most useful for generalizing the prediction, by removing the unpredictable observation noise. The significance of PredPCA was experimentally confirmed by its successful predictions of the 30°–150° rotated images of previously unseen test objects (**Fig. 3a**, middle row; see also **Supplementary Movie S1** for predictions of 90° rotated images, where the right-hand-side images are the predictions of the corresponding true images on the left-hand side). The following ICA separated the extracted components averaged over  $u_{t+30|t}, \dots, u_{t+150|t}$  into a sparse representation, each dimension of which expresses a feature of objects (**Fig. 3b**, top). Applying an additional PCA to the deviation of the extracted component (i.e.,  $u_{t+90|t}$ ) from the average provided the angle of 3D objects as the first principal component (**Fig. 3c**, left). Here, the neural activity predicted the angle of 90° rotated future images, indicating that when observing an asymmetric object (as opposed to a cylindrical object), the network was able to anticipate whether its image would be wider or narrower after 90° rotation. Notably, these prediction and feature extraction capabilities were largely retained even in the presence of an artificially added large (white Gaussian) observation noise whose variance had the same magnitude as the variance of original images, demonstrating that the outcomes of PredPCA are highly robust to this noise (**Fig. 3a,b**, bottom, and **Fig. 3c**, right; see also **Supplementary Movie S2** for predictions of 90° rotated

images). The optimal encoding dimensionality for a network trained with images containing the artificial noise was smaller than that for a network trained with the original images (**Fig. 3d**), indicating that the sampling fluctuation caused by the observation noise disturbed the prediction of minor components. We confirmed an earlier decrease of the test prediction error for PredPCA with the number of training samples, compared with the naïve AR model and SSMS based on Kalman or Bayesian filter [11,13] (**Fig. 3e**). The early convergence of PredPCA's test prediction error implies that PredPCA has already achieved its asymptotic best accuracy based exclusively on the limited number of given training data, because no further error reduction is expected with additional training data once the error converged—owing to the convexity of PredPCA and the fact that the generalization error is inversely proportional to the number of training samples. In short, PredPCA successfully extracted information of object features and rotation as the most informative components for predictions, with little influence of the observation noise level. Subsequently, it successfully predicted future images of objects with the minimum test error even with the shortage of training data, highlighting that PredPCA determined the plausible rule for rotating generic objects.

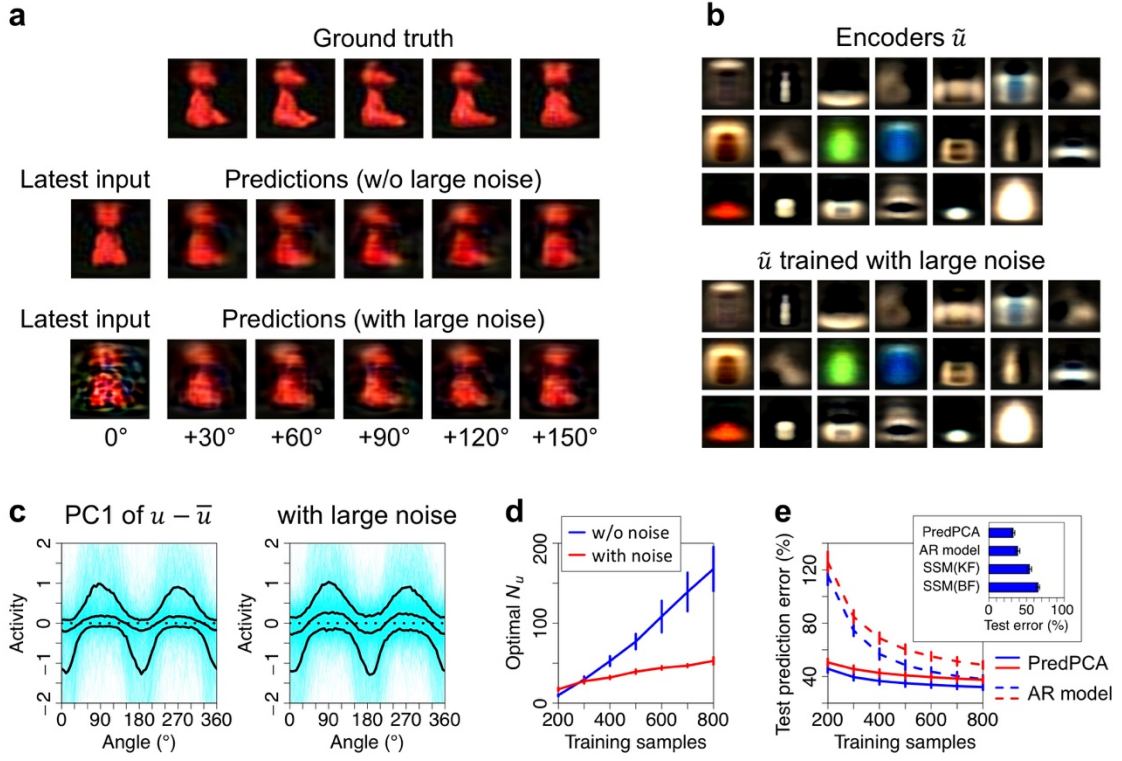


**Figure 3.** PredPCA-based denoising, hidden state extraction, and subsequent input prediction of movies of rotating 3D objects. **(a)** Snapshots of the prediction results. Latest input image (furthest left) and true (top) and predicted images after 30°, 60°, 90°, 120°, and 150° rotations, without (middle row) and with (bottom) artificially added observation noise. **(b)** Images corresponding to 20-dimensional sparse representations ( $\tilde{u}_t$ ) each expressing a feature of objects. These images were obtained by applying ICA with super-Gaussian prior distribution to the first 20 principal components of PredPCA, averaged over different prediction points  $\bar{u}_t = (u_{t+30|t} + \dots + u_{t+150|t})/5$ . These images visualize linear mappings from each independent component to the observation. **(c)** Rotation of objects encoded in the first principal component of the baseline-subtracted encoding states of  $u_{t+90|t}$  (i.e.,  $u_{t+90|t} - \bar{u}_t$ ). Black lines indicate 20, 50, and 80 percentiles, whereas cyan lines show trajectories for each object. **(d)** Optimal encoding dimensionality increasing with training sample size, in the absence (blue) and presence (red) of the

large observation noise. (e) Comparison of test prediction error, defined by  $error_k \equiv \langle |g_{t+k} - W^T u_{t+k|t}|^2 \rangle / \langle |g_{t+k}|^2 \rangle$ , where  $g_t \equiv s_t - \omega_t$  indicates the observation-noise-free input. PredPCA (solid lines) show a smaller test prediction error and an earlier error convergence compared with the naïve AR model (dashed lines). Blue and red lines denote the error in the absence and presence of the large observation noise. Inset panel depicts the comparison of test prediction error between PredPCA, naïve AR model, and SSM based on Kalman filter (KF) and Bayesian filter (BF), when trained with 800 objects in the absence the noise. (d)(e) are obtained with 10 different realizations of training and test samples. The error bars indicate the standard deviation. See Method G for further details.

As a further application to more natural data, we lastly trained a neural network with natural scenes viewed from a driving car [35] (**Fig. 4** and **Supplementary Movie S3**). Here, our motivation was not to compare the prediction accuracy of PredPCA with that of state-of-the-art video prediction methods exploiting engineering wisdom, but to demonstrate the applicability of our simple analytically-solvable linear method to real-world video prediction tasks, while persisting the global convergence and true system identification guarantees. We separated movies into six groups of data based on the driving speed of a car and trained six networks separately with each data through PredPCA (see Method G for the detail). A movie made by synthesizing the outcomes of the six networks successfully predicted the 0.5 s future images of previously unexperienced natural scenes (**Fig. 4**, second row). We confirmed that the error between the true future images

and the predictions (**Fig. 4**, fourth row) was 70% of that between the true future images and the latest input images (**Fig. 4**, bottom). This result indicates that, although any unexpected events during the 0.5 s were definitely unpredictable and some predictions were failed owing to the limited effective dimensionality of the input, PredPCA could provide predictions that interpolate between the unseen future images and the latest input images, without using any label for training. Those results highlight the PredPCA’s generalization capability and wide applicability to real-world data.



**Figure 4.** PredPCA of natural scene movies. Four examples are shown. Top: Ground truth or target image ( $s_{t+15}$ ); i.e., 0.5 s future of latest input with 30 frames per second. Second row: Predicted image using PredPCA ( $W^T u_{t+15|t}$ ). Note that blurry edges in predicted images were mostly because PredPCA predicted the mean of future outcome images. Third row: Latest input image ( $s_t$ ). Fourth row: Prediction error between grand truth and predicted images, where whiteness

indicates the amount of the error (magnitude of  $s_{t+15} - W^T u_{t+15|t}$ ). Bottom: Deviation between grand truth and latest input images (magnitude of  $s_{t+15} - s_t$ ). See Method G for further details.

## DISCUSSION

Our proposed scheme, PredPCA, was shown to identify a concise representation that provides the global minimum of the test prediction error, by first predicting subsequent observations and then performing post-hoc PCA of the predicted inputs. The analytical expression of the test prediction error (Equation (7)) enables us to understand the mechanism of how the sampling fluctuation disturbs the generalization of prediction. From this perspective, an input is decomposed into predictable information and unpredictable noise, where only the latter generates the sampling fluctuation and thus causes entropy (i.e., generalization error) [23]. PredPCA can effectively filter out unpredictable noise, prevent the intake of entropy into the network, and consequently improve the information quality within the network. This is essential for maximizing the prediction generalization capability, as well as for ensuring the accurate and unbiased estimation of true system properties, comprising hidden states, system parameters, and dimensionalities. Our scheme is formally based on Akaike's statistics [14,23] and is consistent with existing information theoretical views of biological optimizations, including maximum negentropy [36], predictive coding [1,2], predictive information [37], and the free energy principle [38,39]—providing them a normative, analytically-solvable example of a neural network that maximizes information quality and generalization capability.

Conventional prediction strategies using autoencoders [8,9] or SSMs [11–13] fail to provide an accurate prediction depending on the initial condition or noise level, as shown in **Figs. 2 and 3** and Methods C. In contrast, PredPCA is a convex optimization. It comprises a preceding AR model that filters out the observation noise and a post-hoc PCA that reduces the generalization error (Equation (7) and Methods D). This approach guarantees the reliable identification of the true system with a global convergence guarantee (Methods E, F and **Table 2**). The outcomes of PredPCA are also useful as a plausible initial condition or an empirical prior for other methods. The improvement of generalization capability by omitting minor eigenmodes has been reported using deep neural networks [40,41], implying a potential extension of PredPCA to analytically solve the optimal representations for deep learning in a weakly nonlinear regime.

In terms of model selection schemes, conventional brute force model comparisons, such as those based on some information criterion [14–16] or cross-validation [17], may identify the true system properties after a combinatorially large number of iterations, by searching all possible subsets of the full model. However, these approaches are not practical for large-scale system prediction, as the computational complexity increases exponentially with the system size. In contrast, the computational complexity of PredPCA for identifying true system properties increases merely as the cubic order of the system size (owing to the cost of eigenvalue decomposition), highlighting the advantage of PredPCA for processing big data.

PredPCA-type learning can be implemented in biological neuronal networks and biologically inspired neuromorphic chips [42,43]. Neurons in these systems must update their synapses to

perform predictions under physiological or physical constraints—in particular, it is difficult for them to access non-local information, such as the synaptic weights of other neurons [44]. This fact limits biologically plausible learning to be a local rule that updates synapses based on and only on pre- and post-synaptic neural activities and additional directly accessible signals. As conventional PCA and ICA algorithms are non-local, we have developed a local learning algorithm that performs both PCA and ICA [45–47]. This algorithm can make PredPCA a local learning rule and guarantees its biological plausibility. Hence, one can speculate that PredPCA-type learning underlies the generalization capability of biological organisms.

From the perspective of generalizing prediction, the formula of the test prediction error expectation (Equation (7)) claims that a predictor should utilize a low-dimensional internal model [48] at an early learning stage, and gradually grow its dimensionality to imitate the true system that generates sensory data. One can associate this property with the adaptation in biological organisms during their lifetime or over evolution, implying that the emergence, growth, and adaptation of an organism’s internal model may be a corollary of the simple principle of test prediction error minimization. According to this theory, it would be beneficial to have some neuronal substrate, such as neuromodulators [49,50], to encode the test prediction error expectation for mediating structural learning or model selection in the brain.

In summary, PredPCA was proven to be an analytically solvable unsupervised dimensionality reduction scheme capable of extracting the most informative components for generalizing prediction. By effectively filtering out unpredictable noise, PredPCA can reliably identify true



system properties, with a global convergence guarantee, and can globally minimize the test prediction error. Although this paper focuses on the autoregression, PredPCA can minimize the generalization error for a class of regression tasks, indicating its potential applicability to various real-world applications. As a mathematically-proven optimal generalization strategy, our scheme is potentially useful for understanding biological generalization mechanisms and creating artificial general intelligence.

## **Acknowledgements**

This work was supported by RIKEN Center for Brain Science (T.I. and T.T.), Brain/MINDS from AMED under Grant Number JP19dm020700 (T.T.), and JSPS KAKENHI Grant Number JP18H05432 (T.T.). The funders had no role in the study design, data collection and analysis, decision to publish, or preparation of the manuscript.

## **Author Contributions**

Takuya Isomura conceived and designed PredPCA, performed the mathematical analyses and simulations, and wrote the manuscript. Taro Toyozumi supervised T.I. from the early state of this work, confirmed rigor of the mathematical analyses, and wrote the manuscript.

## Additional Information

**Competing Interests:** The authors declare that they have no competing interests.

## References

1. Rao, R. P. & Ballard, D. H. Predictive coding in the visual cortex: a functional interpretation of some extra-classical receptive-field effects. *Nat. Neurosci.* **2**, 79-87 (1999).
2. Friston, K. A theory of cortical responses. *Philos. Trans. R. Soc. Lond. B Biol. Sci.* **360**, 815-836 (2005).
3. Mathieu, M., Couprie, C. & LeCun, Y. Deep multi-scale video prediction beyond mean square error. Preprint at <https://arxiv.org/abs/1511.05440> (2015).
4. Lotter, W., Kreiman, G. & Cox, D. Deep predictive coding networks for video prediction and unsupervised learning. Preprint at <https://arxiv.org/abs/1605.08104> (2016).
5. Hurvich, C. M. & Tsai, C. L. Regression and time series model selection in small samples. *Biometrika* **76**, 297-307 (1989).
6. Hurvich, C. M. & Tsai, C. L. A corrected Akaike information criterion for vector autoregressive model selection. *J. Time Series Anal.* **14**, 271-279 (1993).
7. Cunningham, J. P. & Ghahramani, Z. Linear dimensionality reduction: Survey, insights, and generalizations. *J. Mach. Learn. Res.* **16**, 2859-2900 (2015).

8. Hinton, G. E. & Salakhutdinov, R. R. Reducing the dimensionality of data with neural networks. *Science* **313**, 504-507 (2006).
9. Kingma, D. P. & Welling, M. Auto-encoding variational bayes. Preprint at <https://arxiv.org/abs/1312.6114> (2013).
10. Hochreiter, S. & Schmidhuber, J. Long short-term memory. *Neural Comput.* **9**, 1735-1780 (1997).
11. Kalman, R. E. A new approach to linear filtering and prediction problems. *J. Basic Eng.* **82**, 35-45 (1960).
12. Julier, S. J. & Uhlmann, J. K. New extension of the Kalman filter to nonlinear systems. In *Signal processing, sensor fusion, and target recognition VI* (Vol. 3068, pp. 182-193). (International Society for Optics and Photonics, 1997).
13. Friston, K. J., Trujillo-Barreto, N. & Daunizeau, J. DEM: A variational treatment of dynamic systems. *NeuroImage* **41**, 849-885 (2008).
14. Akaike, H. A new look at the statistical model identification. *IEEE Trans. Automat. Contr.* **19**, 716-723 (1974).
15. Murata, N., Yoshizawa, S. & Amari, S. I. Network information criterion-determining the number of hidden units for an artificial neural network model. *IEEE Trans. Neural Netw.* **5**, 865-872 (1994).

16. Schwarz, G. Estimating the dimension of a model. *Ann. Stat.* **6**, 461-464 (1978).
17. Arlot, S. & Celisse, A. A survey of cross-validation procedures for model selection. *Stat. Surv.* **4**, 40-79 (2010).
18. Belouchrani, A., Abed-Meraim, K., Cardoso, J. F. & Moulines, E. A blind source separation technique using second-order statistics. *IEEE Trans. Signal Process.* **45**, 434-444 (1997).
19. Cichocki, A., Zdunek, R., Phan, A. H. & Amari, S.I. Nonnegative matrix and tensor factorizations: applications to exploratory multi-way data analysis and blind source separation. (West Sussex, UK: John Wiley & Sons, 2009).
20. Comon, P. & Jutten, C. (Eds.). Handbook of Blind Source Separation: Independent component analysis and applications. (Academic press, 2010).
21. Ljung, L. System Identification: Theory for the User (2nd ed.). (Prentice-Hall, 1999).
22. Schoukens, J. & Ljung, L. Nonlinear System Identification: A User-Oriented Roadmap. Preprint at <https://arxiv.org/abs/1902.00683> (2019).
23. Akaike, H. Prediction and entropy. In *Selected Papers of Hirotugu Akaike* (pp. 387-410). (Springer, 1985).
24. Pearson, K. On lines and planes of closest fit to systems of points in space. *Philos. Mag.* **2**, 559-572 (1901).
25. Oja, E. Simplified neuron model as a principal component analyzer. *J. Math. Biol.* **15**, 267-273

(1982).

26. Oja, E. Neural networks, principal components, and subspaces. *Int. J. Neural Syst.* **1**, 61-68 (1989).
27. Xu, L. Least mean square error reconstruction principle for self-organizing neural-nets. *Neural Netw.* **6**, 627-648 (1993).
28. Chen, T., Hua, Y. & Yan, W. Y. Global convergence of Oja's subspace algorithm for principal component extraction. *IEEE Trans. Neural Netw.* **9**, 58-67 (1998).
29. Comon, P. Independent component analysis, a new concept? *Signal Process.* **36**, 287-314 (1994).
30. Bell, A. J. & Sejnowski, T. J. An information-maximization approach to blind separation and blind deconvolution. *Neural Comput.* **7**, 1129-1159 (1995).
31. Amari, S. I., Cichocki, A. & Yang, H. H. A new learning algorithm for blind signal separation. *Adv. Neural Info. Proc. Syst.* **8**, 757-763 (1996).
32. The MNIST data set is available at <http://yann.lecun.com/exdb/mnist/index.html>.
33. Isomura, T. & Toyoizumi, T. On the achievability of blind source separation for high-dimensional nonlinear source mixtures. Preprint at <https://arxiv.org/abs/1808.00668> (2018).
34. Geusebroek, J. M., Burghouts, G. J. & Smeulders, A. W. The Amsterdam library of object

images. *Int. J. Comput. Vis.* **61**, 103-112 (2005). The ALOI data set is available at <http://aloi.science.uva.nl>.

35. Yu, F., Xian, W., Chen, Y., Liu, F., Liao, M., Madhavan, V. & Darrell, T. BDD100K: A diverse driving video database with scalable annotation tooling. Preprint at <https://arxiv.org/abs/1805.04687> (2018). The BDD100K data set is available at <https://bdd-data.berkeley.edu>.
36. Schrödinger, E. What is life? The physical aspect of the living cell and mind. (Cambridge University Press, 1944).
37. Palmer, S. E., Marre, O., Berry, M. J. & Bialek, W. Predictive information in a sensory population. *Proc. Natl. Acad. Sci. USA* **112**, 6908-6913 (2015).
38. Friston, K., Kilner, J. & Harrison, L. A free energy principle for the brain. *J. Physiol. Paris* **100**, 70-87 (2006).
39. Friston, K. The free-energy principle: a unified brain theory? *Nat. Rev. Neurosci.* **11**, 127-138 (2010).
40. Suzuki, T., Abe, H., Murata, T., Horiuchi, S., Ito, K., Wachi, T., ... & Nishimura, T. Spectral-Pruning: Compressing deep neural network via spectral analysis. Preprint at <https://arxiv.org/abs/1808.08558> (2018).
41. Oymak, S., Fabian, Z., Li, M. & Soltanolkotabi, M. Generalization Guarantees for Neural Networks via Harnessing the Low-rank Structure of the Jacobian. Preprint at <https://arxiv.org/abs/1906.05392> (2019).

42. Neftci, E. Data and power efficient intelligence with neuromorphic learning machines. *iScience* **5**, 52-68 (2018).
43. Fouda, M., Neftci, E., Eltawil, A. M. & Kurdahi, F. Independent component analysis using RRAMs. *IEEE Trans. Nanotech.* **18**, 611-615 (2018).
44. Lee, T. W., Girolami, M., Bell, A. J. & Sejnowski, T. J. A unifying information-theoretic framework for independent component analysis. *Comput. Math. Appl.* **39**, 1-21 (2000).
45. Isomura, T. & Toyoizumi, T. A local learning rule for independent component analysis. *Sci. Rep.* **6**, 28073 (2016).
46. Isomura, T. & Toyoizumi, T. Error-gated Hebbian rule: A local learning rule for principal and independent component analysis. *Sci. Rep.* **8**, 1835 (2018).
47. Isomura, T. & Toyoizumi, T. Multi-context blind source separation by error-gated Hebbian rule. *Sci. Rep.* **9**, 7127 (2019).
48. Dayan, P., Hinton, G. E., Neal, R. M. & Zemel, R. S. The Helmholtz machine. *Neural Comput.* **7**, 889-904 (1995).
49. Frémaux, N. & Gerstner, W. Neuromodulated spike-timing-dependent plasticity, and theory of three-factor learning rules. *Front. Neural Circuits* **9**, 85 (2016).
50. Kuśmierz, Ł., Isomura, T. & Toyoizumi, T. Learning with three factors: modulating Hebbian plasticity with errors. *Curr. Opin. Neurobiol.* **46**, 170-177 (2017).

## METHODS

In what follows, we mathematically express the benefits of PredPCA. Methods A and B formally define the system and PredPCA. Methods C and D prove that PredPCA inherits preferable properties of both the standard PCA and AR models, and outperforms naïve PCA and AR models in the robustness to noise and generalization of prediction. Methods E and F demonstrate that PredPCA identifies the optimal hidden state estimator and the true system parameters with a global convergence guarantee, owing to asymptotic property of linear neural networks with high-dimensional inputs [33]. Methods G provides the simulation protocols.

### A. System

We suppose that in the external world a system is expressed as  $x_{t+1} = f_t + z_t$  and  $s_t = g_t + \omega_t$  with mutually independent white Gaussian noises  $z_t \sim \mathcal{N}[0, \Sigma_z]$  and  $\omega_t \sim \mathcal{N}[0, \Sigma_\omega]$ , where  $f_t \equiv f(x_t, x_{t-1}, \dots)$  and  $g_t \equiv g(x_t)$  are nonlinear functions of  $x_t$ . We assume that the system is in a steady state. To generate predictable dynamics,  $\Sigma_z$  is assumed to be smaller than  $\Sigma_x$  in magnitude; whereas, we typically consider a large  $\Sigma_\omega$ . Without loss of generality, we can suppose that the steady state of  $x_t$  follows a distribution with zero mean and the identity covariance  $\Sigma_x \equiv I$ . For analysis, we consider a family of functions  $f_t \equiv B\psi_t$  and  $g_t \equiv A\psi_t$  spanned by nonlinear basis functions  $\psi_t \equiv \psi(x_t) \in \mathbb{R}^{N_\psi}$ , where  $N_\psi$  is defined as the number of linearly



independent bases,  $B \in \mathbb{R}^{N_x \times N_\psi}$  is a full-row-rank transition matrix, and  $A \in \mathbb{R}^{N_s \times N_\psi}$  is a full-column-rank mapping matrix from the bases to the sensory input. Thus, Equation (1) becomes

$$s_t = A\psi_t + \omega_t \quad (8)$$

and Equation (2) becomes

$$x_{t+1} = B\psi_t + z_t. \quad (9)$$

As the dimensions and variety of bases increase, each element of  $f(x_t)$  and  $g(x_t)$  asymptotically expresses an arbitrary nonlinear mapping if  $A$  and  $B$  are suitably selected. We assume  $N_x \leq N_\psi \leq N_s$  such that the system dynamics are produced by hidden states lower-dimensional than the observations. Although this paper supposes  $\psi_t = \psi(x_t)$ , the same analysis can be applied to a system comprising  $\psi_t = \psi(x_t, x_{t-1}, \dots)$  by redefining  $(x_t, x_{t-1}, \dots)$  and  $(s_t, s_{t-1}, \dots)$  as new  $x_t$  and  $s_t$ , respectively. **Table 1** presents the glossary of expressions.

## B. Derivation of PredPCA

PredPCA aims to minimize the multistep prediction error for predicting 1 to  $K_f$ -step future of the above-mentioned system by optimizing synaptic matrices using and only using the current and past observations  $s_t, s_{t-1}, \dots, s_{t-K_p+1}$ , where  $K_f$  and  $K_p$  are imposed by the problem setup. Hidden states and bases  $(x_t, \psi_t)$ , all system parameters  $(A, B, \Sigma_x, \Sigma_\psi, \Sigma_z, \Sigma_\omega)$ , and the numbers of hidden state and basis dimensions  $(N_x, N_\psi)$  are unknown to a learner.

The error for predicting the  $k$ -step future is defined by  $\varepsilon_{t+k|t} \equiv s_{t+k} - W^T V_k \phi_t$ , where  $\phi_t \equiv (s_t^T, s_{t-1}^T, \dots, s_{t-K_p+1}^T)^T \in \mathbb{R}^{N_\phi}$  is a vector of observations,  $W \in \mathbb{R}^{N_u \times N_s}$  is the transpose of the decoding synaptic weight matrix, and  $V_k \in \mathbb{R}^{N_u \times N_\phi}$  is the  $k$ -th encoding synaptic weight matrix. Although general nonlinear bases can be used as  $\phi_t$ , a simple vector of observations serves the purpose of this paper. We will show below that the prediction and system identification using these linear bases are accurate when the dimensions and variety of inputs are sufficiently large. Minimizing  $\varepsilon_{t+k|t}$  can be viewed as a generalization of the standard PCA [27] that minimizes the reconstruction error of the current observation (i.e.,  $\varepsilon_t^{PCA} \equiv s_t - W^T W s_t$ ).

Formally, the cost function of PredPCA for multistep predictions is defined by

$$L \equiv \frac{1}{2} \sum_{k=1}^{K_f} \langle |\varepsilon_{t+k|t}|^2 \rangle_q, \quad (10)$$

where  $\langle \cdot \rangle_q \equiv \frac{1}{T} \sum_{t=1}^T \cdot$  is the expectation over the empirical distribution  $q$ . Solving the fixed point of the above cost function  $L$  with respect to  $V_k$  yields the optimal estimator. From

$$\frac{\partial L}{\partial V_k} = -W \langle \varepsilon_{t+k|t} \phi_t^T \rangle_q = -W \langle (s_{t+k} - W^T V_k \phi_t) \phi_t^T \rangle_q = 0, \quad (11)$$

under an assumption of  $WW^T = I$  (which is preserved by Equation (13) below), the optimal  $V_k$  is found as

$$V_k = W \langle s_{t+k} \phi_t^T \rangle_q \langle \phi_t \phi_t^T \rangle_q^{-1}. \quad (12)$$

We define the maximum likelihood estimator of  $s_{t+k}$  by  $\mathbf{s}_{t+k|t} \equiv \mathbf{Q}_k \phi_t$ , where  $\mathbf{Q}_k \equiv$

$\langle s_{t+k} \phi_t^T \rangle_q \langle \phi_t \phi_t^T \rangle_q^{-1}$  is the optimal (maximum likelihood) matrix estimator. Throughout the

manuscript, a bold case variable (e.g.,  $\mathbf{s}_{t+k|t}$ ) indicates the estimator of the corresponding italic case variable (e.g.,  $s_{t+k}$ ). The  $k$ -th encoder  $u_{t+k|t}$  is thus defined by  $u_{t+k|t} \equiv W\mathbf{s}_{t+k|t}$ . The optimal  $W$  is determined by the gradient descent of  $L$ :

$$\dot{W} \propto -\frac{\partial L}{\partial W} = \sum_{k=1}^{K_f} \left\langle u_{t+k|t} (s_{t+k} - W^T u_{t+k|t})^T \right\rangle_q. \quad (13)$$

Equation (13) is similar to Oja's subspace rule for PCA [25] except that  $\mathbf{s}_{t+k|t}$  is used instead of  $s_{t+k}$  to define  $u_{t+k|t}$ . In this sense, PredPCA conducts post-hoc dimensionality reduction (PCA) of the predicted input. The update by Equation (13) maintains  $W$  as an orthogonal matrix (i.e.,  $WW^T = I$ ) throughout the learning.

The above PredPCA solution can also be obtained by eigenvalue decomposition. When  $WW^T = I$ , the cost function is transformed as  $L = \frac{1}{2} \sum_{k=1}^{K_f} \left\langle |s_{t+k} - W^T W \mathbf{s}_{t+k|t}|^2 \right\rangle_q = \frac{K_f}{2} (\text{tr}[\mathbf{\Sigma}_s] - \text{tr}[W \mathbf{\Sigma}_s W^T])$ , where  $\mathbf{\Sigma}_s \equiv \langle s_t s_t^T \rangle_q$  and  $\mathbf{\Sigma}_s \equiv \frac{1}{K_f} \sum_{k=1}^{K_f} \langle \mathbf{s}_{t+k|t} \mathbf{s}_{t+k|t}^T \rangle_q$  are the actual and predicted input covariances calculated based on the empirical distribution, respectively. Thus, the minimization of  $L$  is achieved by maximizing the second term under the constraint of  $WW^T = I$  (note that this constraint is automatically satisfied by minimizing  $L$ ). Hence, the optimal  $W$  is provided as the transpose of the major eigenvectors of  $\mathbf{\Sigma}_s$ . This solution is unique up to the multiplication of an  $N_u \times N_u$  orthogonal matrix from the left. The global convergence and absence of spurious solutions are also guaranteed when  $W$  is computed by Equation (13) because of the global convergence property of Oja's subspace rule for PCA [26]. In short, PredPCA is a convex optimization and thus it can reliably identify the optimal synaptic matrices  $W$  and

$V_1, \dots, V_{K_f}$  for predictions, which provides the global minimum of the cost function  $L$ .

### C. PredPCA (but not PCA) filters out observation noise

Here, we compare the components extracted using PredPCA and the standard PCA. We show that only PredPCA can remove observation noise and accurately estimate the observation matrix  $A$  as training sample size  $T$  increases.

We introduce the expectation over true distribution  $p(\phi_t, s_{t+1}, \dots, s_{t+K_f})$ , denoted by  $\langle \cdot \rangle \equiv \int \cdot p(\phi_t, s_{t+1}, \dots, s_{t+K_f}) d\phi_t ds_{t+1} \dots ds_{t+K_f}$ . The empirical distribution approaches this true distribution in the large training sample size limit:  $p(\phi_t, s_{t+1}, \dots, s_{t+K_f}) = \text{plim}_{T \rightarrow \infty} q(\phi_t, s_{t+1}, \dots, s_{t+K_f})$ . Throughout the manuscript,  $\langle s_t \rangle = 0$ ,  $\langle \psi_t \rangle = 0$ , and  $\langle x_t \rangle = 0$  are supposed for the sake of simplicity. The true covariance matrix of some variable  $\xi_t$  is denoted by  $\Sigma_\xi \equiv \text{Cov}[\xi_t] \equiv \langle \xi_t \xi_t^T \rangle - \langle \xi_t \rangle \langle \xi_t^T \rangle$ . Here, any estimator or statistic  $\boldsymbol{\theta}$  under consideration, calculated based on the empirical distribution, can be decomposed into its true value  $\theta$  and its generalization error  $\delta\theta \equiv \boldsymbol{\theta} - \theta$ , where  $\delta\theta$  is in the  $T^{-1/2}$  order (see Supplementary Methods S1 for the conditions and the proof). Below, we will decompose  $\boldsymbol{\theta}$  into  $\theta$  and  $\delta\theta$  and then solve  $\theta$  analytically.

The standard PCA conducts the eigenvalue decomposition of the actual input covariance, calculated based on the empirical distribution:  $\Sigma_s \equiv \langle s_t s_t^T \rangle_q$ . From Equation (8), it is decomposed as  $\Sigma_s = \Sigma_s + \mathcal{O}(T^{-1/2}) = A \Sigma_\psi A + \Sigma_\omega + \mathcal{O}(T^{-1/2})$  owing to the independence of  $\psi_t$  and  $\omega_t$ .

As the observation noise covariance  $\Sigma_\omega$  is involved in  $\Sigma_s$ , the major eigenvectors of  $\Sigma_s$  that PCA extracts are biased toward the directions of the noise's major eigenvectors. This bias is a common issue of autoencoding approaches [8,9] that makes the identification of the true system parameters difficult.

In contrast to the standard PCA, PredPCA conducts the eigenvalue decomposition of the predicted input covariance:  $\Sigma_s \equiv \frac{1}{K_f} \sum_{k=1}^{K_f} \langle \mathbf{s}_{t+k|t} \mathbf{s}_{t+k|t}^T \rangle_q$ . Owing to this construction, the identification of system parameters  $(A, B, \Sigma_x, \Sigma_\psi, \Sigma_\omega, \Sigma_z)$  based on PredPCA is not biased by the observation noise. From the independence between  $\omega_{t+k}$  and  $\phi_t$ ,  $\mathbf{s}_{t+k|t} = A \langle \psi_{t+k} \phi_t^T \rangle \Sigma_\phi^{-1} \phi_t + \mathcal{O}(T^{-1/2})$ . Thus, we obtain

$$\Sigma_s = A \Sigma_\psi A^T + \mathcal{O}\left(T^{-\frac{1}{2}}\right), \quad (14)$$

where  $\Sigma_\psi \equiv \frac{1}{K_f} \sum_{k=1}^{K_f} \langle \psi_{t+k} \phi_t^T \rangle \Sigma_\phi^{-1} \langle \phi_t \psi_{t+k}^T \rangle$  is the predicted hidden basis covariance, calculated based on the true distribution. Applying the eigenvalue decomposition to  $\Sigma_s$  provides the set of major eigenvectors  $\mathbf{P}_s \equiv (\mathbf{P}_{.1}, \dots, \mathbf{P}_{.N_\psi}) \in \mathbb{R}^{N_s \times N_\psi}$  that correspond to asymptotically non-zero eigenvalues. Because of the uniqueness of the eigenvalue decomposition,  $\mathbf{P}_s$  converges to matrix  $A$  as the number of training samples increases—up to the multiplication of a full-rank matrix  $\Omega_\psi \in \mathbb{R}^{N_\psi \times N_\psi}$  from the right-hand side. Hence, we refer to  $\mathbf{P}_s$  as the estimator of  $A$ :

$$\mathbf{A} \equiv \mathbf{P}_s = P_s + \mathcal{O}\left(T^{-\frac{1}{2}}\right) = A \Omega_\psi^{-1} + \mathcal{O}\left(T^{-\frac{1}{2}}\right). \quad (15)$$

Here, we introduced the inverse of  $\Omega_\psi$  (instead of  $\Omega_\psi$  itself) for our convenience. Note that  $P_s$  is the set of major eigenvectors of the generalization-error-free predicted input covariance  $\Sigma_s \equiv$

$A\Sigma_\psi A^T$ . In short, PredPCA can identify matrix  $A$  with asymptotically zero error without directly observing  $\psi_t$ . Notably, the number of basis dimensions  $N_\psi$  is also identifiable by counting the number of asymptotically non-zero eigenvalues of  $\Sigma_s$ , which converges to the true  $N_\psi$  for a large training sample size (see Methods D for the formal definition of the estimator  $\mathbf{N}_\psi$  using the test prediction error).

In addition, multiplying  $\mathbf{P}_s^T$  to the predicted input yields the predicted basis estimator:

$$\Psi_{t+k|t} \equiv \mathbf{P}_s^T \mathbf{s}_{t+k|t} = \Omega_\psi \langle \psi_{t+k} \phi_t^T \rangle \Sigma_\phi^{-1} \phi_t + \mathcal{O}\left(T^{-\frac{1}{2}}\right). \quad (16)$$

The last equality holds from the orthogonality of eigenvectors, i.e.,  $P_s^T A = P_s^T P_s \Omega_\psi = \Omega_\psi$ , and the independence between  $\omega_{t+k}$  and  $\phi_t$ . Indeed,  $u_{t+k|t}$  with optimized synaptic matrices is equivalent to  $\Psi_{t+k|t}$  when  $N_u = N_\psi$ . In short, PredPCA can provide the maximum likelihood estimator of the hidden bases without directly observing  $\psi_{t+k}$ —up to the multiplication of the full-rank ambiguity factor  $\Omega_\psi$  from the left-hand side. This ambiguity factor is safely absorbed into the definition of  $\psi_t$  without changing the system dynamics, by applying the following transformations:  $\Omega_\psi \psi_t \rightarrow \psi_t$ ,  $P_s = A\Omega_\psi^{-1} \rightarrow A$ , and  $B\Omega_\psi^{-1} \rightarrow B$ . Therefore, the estimated hidden dynamics are formally homologous to the original dynamics.

#### D. PredPCA (but not AR models) minimizes test prediction error

A learner needs to predict the future consequences of unseen input data, based on learning with a limited number of training samples. Here, we analytically solve the expectation of the

PredPCA's test prediction error, as a function of the training samples ( $T$ ), encoding dimensions ( $N_s$ ), and number of past observations used for prediction ( $N_\phi = K_p N_s$ ). Its minimization enables a learner to maximize the generalization ability by optimizing free parameters in the network, without knowing the true distribution that generates test samples.

PredPCA's test prediction error is defined as the squared error over the true distribution  $p$ .

Meanwhile, the learning is based on the empirical distribution  $q$ ; thus, the test error is given as a functional of  $q$ :

$$L_{test}[q] \equiv \frac{1}{2} \sum_{k=1}^{K_f} \langle |\varepsilon_{t+k|t}[q]|^2 \rangle. \quad (17)$$

Here, the prediction error (which is also a functional of  $q$ ) is given as  $\varepsilon_{t+k|t}[q] \equiv s_{t+k} -$

$\mathbf{P}_s \mathbf{P}_s^T \mathbf{s}_{t+k|t}$  using the major eigenvectors of the predicted input covariance  $\mathbf{P}_s \equiv (\mathbf{P}_{\cdot 1}, \dots, \mathbf{P}_{\cdot N_u}) \in \mathbb{R}^{N_s \times N_u}$  and the maximum likelihood estimator  $\mathbf{s}_{t+k|t} = \langle s_{t+k} \phi_t^T \rangle_q \langle \phi_t \phi_t^T \rangle_q^{-1} \phi_t$  computed based

on the empirical distribution  $q$ . The generalization error of major eigenvectors  $\mathbf{P}_s$  is negligible up

to the leading order (see Supplementary Methods S2 for details). The  $q$ -dependent factor in

$\mathbf{s}_{t+k|t}$  is computed as  $\langle s_{t+k} \phi_t^T \rangle_q \langle \phi_t \phi_t^T \rangle_q^{-1} = (\langle s_{t+k} \phi_t^T \rangle + \delta \langle s_{t+k} \phi_t^T \rangle_q) (\Sigma_\phi + \delta \langle \phi_t \phi_t^T \rangle_q)^{-1} =$

$Q_k + \delta \langle (s_{t+k} - Q_k \phi_t) \phi_t^T \rangle_q \Sigma_\phi^{-1}$  up to the leading order, using the optimal mapping  $Q_k \equiv$

$\langle s_{t+k} \phi_t^T \rangle \Sigma_\phi^{-1}$  (note that  $\delta \langle \cdot \rangle_q \equiv \langle \cdot \rangle_q - \langle \cdot \rangle$ ). Thus, the prediction error becomes  $\varepsilon_{t+k|t}[q] =$

$s_{t+k} - P_s P_s^T Q_k \phi_t - P_s P_s^T \delta \langle (s_{t+k} - Q_k \phi_t) \phi_t^T \rangle_q \Sigma_\phi^{-1} \phi_t$ , where  $P_s \equiv (P_{\cdot 1}, \dots, P_{\cdot N_u}) \in \mathbb{R}^{N_s \times N_u}$

denotes the major eigenvectors of the generalization-error-free predicted input covariance  $\Sigma_s$ .

Then, we compute the expectation of  $L_{test}[q]$  over different empirical distributions  $q$ , given by

$$\mathcal{L} \equiv \mathbb{E}_{\{q\}}[L_{test}[q]]. \quad (18)$$

This is viewed as a variant of AIC [14] and NIC [15]. The expectation over different  $q$  is equivalent to the expectation over  $p$  for a linear term that involves a single  $\delta\langle\cdot\rangle_q$  factor. Hence,

$\mathbb{E}_{\{q\}}[\delta\langle(s_{t+k} - Q_k\phi_t)\phi_t^T\rangle_q] = 0$ . In contrast, a term that comprises the square of  $\delta\langle\cdot\rangle_q$  yields the positive variance through the interaction of the two factors, which is computed as  $\mathbb{E}_{\{q\}}[\delta\langle(s_{t+k} - Q_k\phi_t)\phi_t^T\rangle_q \Sigma_\phi^{-1} \delta\langle(s_{t+k} - Q_k\phi_t)\phi_t^T\rangle_q^T] = \frac{N_\phi}{T} (\Sigma_s - Q_k \Sigma_\phi Q_k^T)$ . Therefore, we find

$$\underbrace{\mathcal{L}_{\text{test error expectation}}}_{\omega} = \underbrace{\frac{K_f}{2} (\text{tr}[\Sigma_s] - \text{tr}[P_s^T \Sigma_s P_s])}_{\text{training error}} + \underbrace{\frac{K_f N_\phi}{2T} \text{tr}[P_s^T (\Sigma_s - \Sigma_s) P_s]}_{\text{generalization error}} + \mathcal{O}\left(T^{-\frac{3}{2}}\right). \quad (19)$$

See Supplementary Methods S2 for the derivation detail. For the practical use, covariances and eigenvectors in Equation (19) are replaced with their estimators:  $\Sigma_s \rightarrow \hat{\Sigma}_s$ ,  $\Sigma_\phi \rightarrow \hat{\Sigma}_\phi$ , and  $P_s \rightarrow \hat{P}_s$ , where  $\mathcal{L}$  does not change by these replacements in the leading order. Since  $\text{tr}[P_s^T (\Sigma_s - \hat{\Sigma}_s) P_s] > 0$ , the generalization error monotonically increases with the dimensionality of the encoders  $N_u$ . Meanwhile, the reduction of the training prediction error becomes small as  $N_u$  increases, and reaches zero for  $N_u > N_\psi$  due to zero eigenvalues of  $\hat{\Sigma}_s$ . Hence, the optimal  $N_u$  that minimizes  $\mathcal{L}$  is less than  $N_s$ .

The optimal encoding dimensionality that minimizes  $\mathcal{L}$  is comparable to the effective dimensionality of true hidden basis dynamics for large  $T$ . Thus,  $\mathbf{N}_\psi \equiv \text{argmin}_{N_u} \mathcal{L}$  provides the estimator of the true hidden basis dimensionality. In particular,  $\mathbf{N}_\psi = N_\psi$  holds when  $T$  is larger than a large finite constant  $T_\psi^c \equiv N_\phi \text{tr}[\Sigma_s - \hat{\Sigma}_s] / (\Lambda_s)_{N_\psi N_\psi}$ , where  $(\Lambda_s)_{N_\psi N_\psi}$  is the  $N_\psi$ -th (i.e., the smallest non-zero) eigenvalue of  $\Sigma_s$ . In contrast, Equation (19) with  $N_u = N_s$  provides the



test prediction error of an AR model that does not consider hidden states:  $\mathcal{L}_{AR} = \frac{K_f}{2} \left( 1 + \frac{N_\phi}{T} \right) \text{tr}[\Sigma_s - \Sigma_s]$ . As some components of  $\Sigma_\omega$  are generally perpendicular to  $P_s$ ,  $\text{tr}[P_s^T(\Sigma_s - \Sigma_s)P_s] < \text{tr}[\Sigma_s - \Sigma_s]$  for  $N_u < N_s$ . This means that the test prediction error of PredPCA with optimal  $N_u$  is smaller than that of AR models. Hereafter, we suppose  $N_u = N_\psi = N_\psi$ .

### E. Asymptotic linearization theorem guarantees PredPCA to find true hidden states with accuracy guarantee

The asymptotic linearization theorem [33] was originally introduced to guarantee accurate extraction of independently and identically distributed hidden sources from its high-dimensional nonlinear transformations. In this paper, we use this theorem to prove that the true hidden state  $x_t \in \mathbb{R}^{N_x}$  is accurately estimated from its unknown nonlinear transformation  $\psi(x_t) = C\rho(Rx_t + r) \in \mathbb{R}^{N_\psi}$  with asymptotically zero element-wise error as  $N_x$  and  $N_\psi/N_x$  diverge. Here, the elements of  $R \in \mathbb{R}^{N_\psi \times N_x}$  and  $r \in \mathbb{R}^{N_\psi}$  are fixed Gaussian random variables independently drawn from  $\mathcal{N}[0, 1/N_x]$ ;  $C \in \mathbb{R}^{N_\psi \times N_\psi}$  is a matrix whose elements are, on average, in the order of  $N_\psi^{-1/2}$ ; and  $\rho(\cdot): \mathbb{R} \mapsto \mathbb{R}$  is an odd nonlinear function, where the correlation between  $\rho(\xi)$  and unit Gaussian variable  $\xi \sim \mathcal{N}[0, 1]$  is not close to zero. When  $N_\psi$  is large, each element of  $\psi(x_t)$  can represent an arbitrary nonlinear mapping of  $x_t$  by adjusting  $C$  [51–54].

The assumption behind the theorem is that: (1) the elements of hidden states  $x_t$  are not strongly dependent on each other (where zero mean and identity covariance matrix are supposed

without loss of generality), in the sense that the average of higher-order correlations of  $x_t$ 's elements asymptotically vanish for large  $N_x$  with less than the order of 1; and that (2) the matrix components of  $C$  that are parallel to  $R$  are not too small compared to the other components (i.e., the mapping is not very close to a singular mapping)—namely, the ratio of the minimum eigenvalue of  $R^T C^T C R$  to the maximum eigenvalue of  $C C^T$  is assumed to be much greater than 1. Note that  $R^T R = \mathcal{O}(N_\psi/N_x)$  is much greater than 1, so that the condition (2) is easily satisfied when  $C$  is nearly independent from  $R$ . The asymptotic linearization theorem states that under these two conditions, covariance  $\Sigma_\psi$  has a clear spectrum gap that separates major and minor components, and those components correspond to linear and nonlinear transformations of the true hidden states, respectively.

Let  $P \in \mathbb{R}^{N_\psi \times N_x}$  be the set of the first to  $N_x$ -th major eigenvectors of  $\Sigma_\psi$ , and  $\Lambda \in \mathbb{R}^{N_x \times N_x}$  be the diagonal matrix of the corresponding eigenvalues. The asymptotic linearization theorem proved that applying PCA to  $\psi(x_t)$  provides accurate estimation of  $x_t$  up to the multiplication of a fixed orthogonal matrix  $\Omega$ ; i.e.,  $\Lambda^{-1/2} P^T \psi(x_t) = \Omega x_t + \mathcal{O}(\sigma_x)$ . Here,  $\sigma_x =$

$\sqrt{(\overline{\rho^2} - \overline{\rho'}^2) \cdot N_x/N_\psi + \overline{\rho'''}^2/N_x}$  is the standard deviation of the linearization error, where  $\overline{\rho^2} \equiv \int \rho^2(\xi) p(\xi) d\xi$ ,  $\overline{\rho'} \equiv \int \frac{d\rho(\xi)}{d\xi} p(\xi) d\xi$ , and  $\overline{\rho'''} \equiv \int \frac{d^3\rho(\xi)}{d\xi^3} p(\xi) d\xi$  are statistics of the nonlinear function  $\rho$  over unit Gaussian variable  $\xi$ . The linearization error monotonically decreases as the system size increases (i.e., when  $N_\psi/N_x$  and  $N_x$  diverge)—asymptotically achieving the zero-element-wise-error hidden state estimation in the large system size limit.

This theorem can be applied to the estimator of  $\psi(x_t)$ . Let  $\mathbf{P}_\psi \in \mathbb{R}^{N_\psi \times N_x}$  be the major

eigenvectors of  $\Sigma_\psi$  (see Equation (23) below for its definition and analytical solution), and  $\Lambda_\psi \in \mathbb{R}^{N_x \times N_x}$  be the corresponding eigenvalues. The hidden state estimator is defined as

$$\mathbf{x}_{t+k|t} \equiv \Lambda_\psi^{-\frac{1}{2}} \mathbf{P}_\psi^T \Psi_{t+k|t} = \Lambda_\psi^{-\frac{1}{2}} P_\psi^T \Omega_\psi \langle \psi_{t+k} \phi_t \rangle \Sigma_\phi^{-1} \phi_t + \mathcal{O}\left(T^{-\frac{1}{2}}\right). \quad (20)$$

From the asymptotic linearization theorem,  $\Lambda_\psi^{-1/2} P_\psi^T \Omega_\psi \psi_{t+k} = \Omega_x x_{t+k} + \mathcal{O}(\sigma_x)$  holds, where  $\Omega_x \in \mathbb{R}^{N_x \times N_x}$  is a fixed orthogonal matrix. Here, we treated  $\Omega_\psi \psi_{t+k}$  as a nonlinear function of  $x_{t+k}$  and applied the theorem. Thus, Equation (20) is solved analytically as

$$\mathbf{x}_{t+k|t} = \Omega_x \langle x_{t+k} \phi_t \rangle \Sigma_\phi^{-1} \phi_t + \mathcal{O}\left(T^{-\frac{1}{2}}\right) + \mathcal{O}(\sigma_x). \quad (21)$$

This result shows that the maximum likelihood estimator of  $x_{t+k}$  based on  $\phi_t, \langle x_{t+k} \phi_t \rangle \Sigma_\phi^{-1} \phi_t$ , is available (up to the ambiguity factor of  $\Omega_x$  and the order  $T^{-1/2}$  and  $\sigma_x$  small residual terms), despite the fact that PredPCA is unsupervised learning that does not use any explicit data of  $x_{t+k}$  for training. Similar to  $\Omega_\psi$ , the ambiguity of  $\Omega_x$  can be absorbed into the definition of  $x_t$ , without changing any system dynamics, by applying the following transformations:  $\Omega_x x_t \rightarrow x_t$ ,  $\Omega_x B \rightarrow B$ ,  $\Omega_x z_t \rightarrow z_t$ , and  $R \Omega_x^{-1} \rightarrow R$ . Notably, the number of state dimensions  $N_x$  is also identifiable by defining the estimator  $\mathbf{N}_x$  as the largest spectrum gap of  $\Sigma_\psi$ , which is guaranteed to converge to true  $N_x$  when  $\sigma_x$  is smaller than a small positive constant  $\sigma_x^c$  and  $T$  is larger than a large finite constant  $T_x^c$ .

## F. PredPCA identifies true system parameters with an accuracy guarantee

We showed above that PredPCA can identify the true observation matrix  $A$ . Here, we show that

it can also identify all other system parameters  $B$ ,  $\Sigma_\psi$ ,  $\Sigma_x$ ,  $\Sigma_\omega$ , and  $\Sigma_z$  asymptotically—if the assumptions of the asymptotic linearization theorem are met and the number of training samples is large.

Those parameter identifications are based on the linearized transition mapping from  $\psi_t$  to  $\psi_{t+1}$ , denoted by  $\Psi$ ; thus, we first compute the estimator of  $\Psi$ . We decompose  $\psi_{t+1}$  as  $\psi_{t+1} = \Psi\psi_t + \Delta\psi_{t+1|t} + \mathcal{O}(z_t)$ , where  $\Psi = \langle \psi_{t+1}\psi_t^T \rangle \Sigma_\psi^{-1}$  is the optimal basis transition matrix,  $\Delta\psi_{t+1|t}$  is the linearization error that is perpendicular to both  $\psi_t$  and  $z_t$ , and  $\mathcal{O}(z_t)$  is a term related to small noise  $z_t$ . This  $\Psi$  can be viewed as a finite basis size version of Koopman operator [55,56]. The basis estimator based on the current input is defined by  $\Psi_{t|t} \equiv \mathbf{P}_s^T s_t = \Omega_\psi \psi_t + P_s^T \omega_t + \mathcal{O}(T^{-1/2})$ . Using this, we have  $\langle \Psi_{t+k|t+k} \Psi_{t|t}^T \rangle_q = \langle (\Omega_\psi \psi_{t+k} + P_s^T \omega_{t+k})(\Omega_\psi \psi_t + P_s^T \omega_t)^T \rangle + \mathcal{O}(T^{-1/2}) = \Omega_\psi \langle \psi_{t+k} \psi_t^T \rangle \Omega_\psi^T + \mathcal{O}(T^{-1/2})$  as the observation noise is white and independent of  $\psi_t$  and  $\psi_{t+k}$ . In particular,  $\langle \psi_{t+1} \psi_t^T \rangle = \Psi \Sigma_\psi$  and  $\langle \psi_{t+2} \psi_t^T \rangle = \Psi^2 \Sigma_\psi + \langle \Delta\psi_{t+2|t+1} \psi_t^T \rangle$  hold. Thus, we obtain the following estimator of the basis transition matrix:

$$\begin{aligned} \Psi &\equiv \langle \Psi_{t+2|t+2} \Psi_{t|t}^T \rangle_q \langle \Psi_{t+1|t+1} \Psi_{t|t}^T \rangle_q^{-1} = \Omega_\psi \Psi \Omega_\psi^{-1} + \Omega_\psi \langle \Delta\psi_{t+2|t+1} \psi_t^T \rangle \Sigma_\psi^{-1} \Psi^{-1} \Omega_\psi^{-1} + \mathcal{O}\left(T^{-\frac{1}{2}}\right) \\ &= \Omega_\psi \Psi \Omega_\psi^{-1} + \mathcal{O}\left(T^{-\frac{1}{2}}\right) + \mathcal{O}(\sigma_\psi). \end{aligned} \quad (22)$$

This estimator converges to the true  $\Psi$  up to the ambiguity of  $\Omega_\psi$ . The variance of the linearization error term  $\mathcal{O}(\sigma_\psi)$  is in the same order as the variance of nonlinearly transformed components of  $x_t$  that are involved in  $\psi_t$ ; thus, using the asymptotic linearization theorem [33], we compute the variance of the nonlinear components and obtain  $\sigma_\psi = \sqrt{(\overline{\rho^2} - \overline{\rho'}^2)/N_\psi}$  as the

order (see Supplementary Methods S3 for the detail).

Next, we compute the covariance matrices of hidden bases and observation noise. By multiplying the inverse of  $\Psi$  with  $\langle \Psi_{t+1|t+1} \Psi_{t|t}^T \rangle_q = \Omega_\psi \Psi \Sigma_\psi \Omega_\psi^T + \mathcal{O}(T^{-1/2})$ , we find the hidden basis covariance estimator (symmetrized version) as

$$\Sigma_\psi \equiv \frac{1}{2} \left( \Psi^{-1} \langle \Psi_{t+1|t+1} \Psi_{t|t}^T \rangle_q + \langle \Psi_{t|t} \Psi_{t+1|t+1}^T \rangle_q \Psi^{-T} \right) = \Omega_\psi \Sigma_\psi \Omega_\psi^T + \mathcal{O}(T^{-\frac{1}{2}}) + \mathcal{O}(\sigma_\psi). \quad (23)$$

See Supplementary Methods S3 for the order of the linearization error term. Using this  $\Sigma_\psi$ , the observation noise covariance estimator is given as

$$\Sigma_\omega \equiv \Sigma_s - \mathbf{A} \Sigma_\psi \mathbf{A}^T = \Sigma_s - \mathbf{A} \Sigma_\psi \mathbf{A}^T + \mathcal{O}(T^{-\frac{1}{2}}) + \mathcal{O}(\sigma_\psi) = \Sigma_\omega + \mathcal{O}(T^{-\frac{1}{2}}) + \mathcal{O}(\sigma_\psi). \quad (24)$$

Finally, we estimate the state transition matrix and covariance matrices of hidden states and process noise. From Equation (9) and the independence between  $z_{t+2}$  and  $\phi_t$ ,  $\langle x_{t+2} \phi_t^T \rangle = B \langle \psi_{t+1} \phi_t^T \rangle$  holds. Thus, Equation (21) for  $k = 2$  becomes  $\mathbf{x}_{t+2|t} = (\Omega_x B \Omega_\psi^{-1}) \Omega_\psi \langle \psi_{t+1} \phi_t \rangle \Sigma_\phi^{-1} \phi_t + \mathcal{O}(T^{-1/2}) + \mathcal{O}(\sigma_x)$ . Hence, using Equation (16), we find the following estimator of the transition matrix:

$$\mathbf{B} \equiv \langle \mathbf{x}_{t+2|t} \Psi_{t+1|t}^T \rangle_q \langle \Psi_{t+1|t} \Psi_{t+1|t}^T \rangle_q^{-1} = \Omega_x B \Omega_\psi^{-1} + \mathcal{O}(T^{-\frac{1}{2}}) + \mathcal{O}(\sigma_x). \quad (25)$$

The hidden state covariance estimator is given by  $\Sigma_x \equiv \Sigma_x \equiv I$  as we defined  $\Sigma_x$  so. Thus, as

Equation (9) yields  $\Sigma_x = B \Sigma_\psi B^T + \Sigma_z$ , the process noise covariance estimator is given by

$$\Sigma_z \equiv \Sigma_x - \mathbf{B} \Sigma_\psi \mathbf{B}^T = \Omega_x \Sigma_z \Omega_x^T + \mathcal{O}(T^{-\frac{1}{2}}) + \mathcal{O}(\sigma_x). \quad (26)$$

In summary, PredPCA could identify all true system parameters  $A$ ,  $B$ ,  $\Psi$ ,  $\Sigma_\psi$ ,  $\Sigma_x$ ,  $\Sigma_\omega$ , and  $\Sigma_z$

with a global convergence guarantee as the system and training sample sizes increase, using noisy observations only—up to the full-rank linear transformations  $(\Omega_\psi, \Omega_x)$  that do not change the system dynamics. The zero-element-wise-error identification of all parameters will be asymptotically achieved when  $N_\psi/N_x$ ,  $N_x$ , and  $T$  diverge. This global convergence guarantee is an advantage of PredPCA compared with conventional system identification approaches [13,57]. If  $\psi(x_t)$  is a linear function of  $x_t$ , the true system becomes a linear system and thus provides  $\sigma_x = \sigma_\psi = 0$ ; hence, PredPCA is guaranteed to identify all true system parameters with zero error as the increasing training samples, when  $N_x \leq N_s$ . **Table 2** summarizes the definitions and analytical solutions of all estimators. Every estimator can be computed by following the definition, where its analytical solution and accuracy have been proven theoretically.

## G. Simulation protocols

**For Fig. 2.** MNIST dataset [32] comprises 60000 images for training and 10000 images for test.

As a preprocessing, PCA was applied to  $28 \times 28$  hand-digit images to obtain 40-dimensional

compressed inputs  $s_t$ . PredPCA was applied based on  $K_p = 40$  step linear bases  $\phi_t =$

$(s_t^T, \dots, s_{t-39}^T)^T$  to predict  $s_{t+1}$ . ICA [31] was applied to 10 major PredPCA components  $(u_{t+1|t})$  to

make them independent of each other, where the obtained independent encoders are denoted by

$\tilde{u}_{t+1|t}$  (**Fig. 1a**, right). Note that no random replacement of a digit or monochrome inversion

occurred for test image sequences. In **Fig. 1e**, the ascending order sequence was predicted by first

estimating the transition matrix  $B \in \mathbb{R}^{10 \times 10}$  from  $\tilde{u}_{t+1|t}$  to  $\tilde{u}_{t+2|t}$  (**Table 2** and Method F) and

then recursively applying it to predict  $\tilde{u}_{t+k|t}$  based on  $\sigma(\tilde{u}_{t+k-1|t})$ , i.e.,  $\tilde{u}_{t+k|t} = \mathbf{B}\sigma(\tilde{u}_{t+k-1|t})$ , where  $\sigma(\cdot)$  indicates a winner-takes-all operation that makes the maximum element one and others zero. This treatment was served to make greedy predictions of the digit sequences by taking only the most probable future digit at each time step. The Fibonacci series was predicted by first estimating the transition matrix  $\tilde{B} \in \mathbb{R}^{10 \times 100}$  from  $\tilde{u}_{t+2|t} \otimes \tilde{u}_{t+1|t}$  to  $\tilde{u}_{t+3|t}$ , where  $\otimes$  indicates the Kronecker product, and then recursively applying it to predict  $\tilde{u}_{t+k|t}$  based on  $\sigma(\tilde{u}_{t+k-1|t}) \otimes \sigma(\tilde{u}_{t+k-2|t})$ , i.e.,  $\tilde{u}_{t+k|t} = \tilde{\mathbf{B}}(\sigma(\tilde{u}_{t+k-1|t}) \otimes \sigma(\tilde{u}_{t+k-2|t}))$ .

**For Fig. 3.** Images of 3D objects rotating clockwise [34] were defined as the input, where  $360^\circ$  rotation was divided into 72 parts (i.e., 1 step corresponds to  $5^\circ$  rotation). The dataset was randomly divided into 800 training objects (57600 images) and 200 test objects (14400 images). The  $144 \times 144 \times 3$ -dimensional RGB image data were first compressed to 300 dimensions to afford input  $s_t$ . PredPCA was applied to extract 150 major principal components ( $u_{t+k|t}$ ) that are the most useful for predicting  $30^\circ$ ,  $60^\circ$ ,  $90^\circ$ ,  $120^\circ$ , and  $150^\circ$  future observations. Those predictions were based on a set of bases that summarizes observations between  $-180^\circ$  and  $0^\circ$ ,  $\phi_t = (s_t^T \Sigma_\omega^{-1} \mathbf{A}, \dots, s_{t-36}^T \Sigma_\omega^{-1} \mathbf{A})^T$ . Here,  $\mathbf{A}^T \Sigma_\omega^{-1} s_t^T$  was used instead of  $s_t^T$  to construct  $\phi_t$  as the former can filter out the observation noise more effectively, where  $\mathbf{A}$  and  $\Sigma_\omega$  were estimated in advance using PredPCA with  $\phi_t = (s_t^T, \dots, s_{t-36}^T)^T$  (Table 2 and Method F). Note that minor components of  $\Sigma_\phi$  were omitted when calculating  $\Sigma_\phi^{-1}$ . SSMs comprised a state prediction step using Kalman filter [11] or Bayesian filter (generalized Gaussian filter) [13] and a parameter estimation step based on the maximum likelihood (a posteriori) estimation, in a form of

expectation-maximization algorithm or dynamic causal modeling (see [13]). SSMs assumed that the rotated images were generated from a linear or nonlinear system. Kalman filter supposed a linear system comprising  $s_t = Ax_t + \omega_t$  and  $x_{t+1} = Bx_t + z_t$ . Bayesian filter supposed a nonlinear system comprising  $s_t = A \tanh(A'x_t + a) + \omega_t$  and  $x_{t+1} = B \tanh(B'x_t + b) + z_t$ , where parameters  $(A, A', a, B, B', b)$  are optimized.

**For Fig. 4.** Natural scenes viewed from a driving car [35] were defined as the input. We used videos with 200 h total length for training and videos with 4 h total length for test (with 30 frames per second). Those videos were down sampled to  $320 \times 160 \times 3$  RGB image data. Top-left, top-right, bottom-left, and bottom-right areas with each RGB color channel were predicted separately. The  $160 \times 80$ -dimensional images were first compressed to 2000 dimensions to afford input  $s_t$ . The video frames were separated into six groups based on the driving speed of car, which was estimated using the change in frames at each time period. For each group, PredPCA was applied based on a set of bases arranged current and past observations  $\phi_t = (s_t^T, \dots, s_{t-3}^T)^T$ , to extract 200 to 1000-dimensional major principal components ( $u_{t+15|t}$ ) that are the most useful for predicting 0.5 s (i.e., 15 frames) future images. Finally, the outcomes of the six networks, denoted by  $\mathbf{s}_{t+15|t}^{(1)}, \dots, \mathbf{s}_{t+15|t}^{(6)}$ , were synthesized to create the resulting prediction. The network with minimum prediction error at time  $t$  was used for predicting  $s_{t+15}$ ; namely,  $\mathbf{s}_{t+15|t} = \sum_{m=1}^6 \gamma_t^{(m)} \mathbf{s}_{t+15|t}^{(m)}$ , where coefficient  $\gamma_t^{(m)}$  was given as  $\gamma_t^{(m)} = 0.9\gamma_{t-1}^{(m)} + 0.1\sigma\left(-\left|s_t - \mathbf{s}_{t|t-15}^{(m)}\right|^2\right)$  using the winner-takes-all operator (1 for  $m$  that provides the maximum or 0 otherwise).



## References

51. Hornik, K., Stinchcombe, M. & White, H. Multilayer feedforward networks are universal approximators. *Neural Netw.* **2**, 359-366 (1989).
52. Barron, A. R. Universal approximation bounds for superpositions of a sigmoidal function. *IEEE Trans. Info. Theory* **39**, 930-945 (1993).
53. Rahimi, A. & Recht, B. Uniform approximation of functions with random bases. In *Proceedings of the 46th Annual Allerton Conference on Communication, Control, and Computing* 555-561 (2008).
54. Rahimi, A. & Recht, B. Weighted sums of random kitchen sinks: Replacing minimization with randomization in learning. *Adv. Neural Info. Process. Sys.* **21**, 1313-1320 (2008).
55. Koopman, B. O. Hamiltonian systems and transformation in Hilbert space. *Proc. Natl. Acad. Sci. USA* **17**, 315-318 (1931).
56. Lusch, B., Kutz, J. N. & Brunton, S. L. Deep learning for universal linear embeddings of nonlinear dynamics. *Nat. Comm.* **9**, 4950 (2018).
57. Ljung, L. Asymptotic behavior of the extended Kalman filter as a parameter estimator for linear systems. *IEEE Trans. Automat. Contr.* **24**, 36-50 (1979).

**Table 1.** Glossary of expressions.

Expression	Description
$s_t$	Observation
$\psi_t$	Hidden bases
$x_t$	Hidden states
$\omega_t$	Observation noise
$z_t$	Process noise
$A$	Observation matrix
$B$	State transition matrix
$\Sigma_s, \Sigma_\psi, \Sigma_x, \Sigma_\omega, \Sigma_z$	Covariance matrices of $s_t, \psi_t, x_t, \omega_t, z_t$
$N_s$	Number of observation dimensions
$N_\psi$	Number of hidden basis dimensions
$N_x$	Number of hidden state dimensions
$u_{t+k t}$	Encoders
$\phi_t$	Basis functions
$V$	Encoding synaptic weight matrix
$W$	Transpose of decoding synaptic weight matrix
$N_u$	Number of encoder dimensions
$N_\phi$	Number of basis dimensions
$\langle \cdot \rangle_q$	Expectation over empirical distribution $q$
$\langle \cdot \rangle$	Expectation over true distribution $p$

**Table 2.** Definitions and analytical solutions of estimators.

Estimator	Definition	Analytical solution
$\mathbf{s}_{t+k t}$	$\langle \mathbf{s}_{t+k} \phi_t^T \rangle_q \langle \phi_t \phi_t^T \rangle_q^{-1} \phi_t$	$\langle \mathbf{s}_{t+k} \phi_t^T \rangle \Sigma_\phi^{-1} \phi_t + \mathcal{O}(T^{-1/2})$
$\Psi_{t+k t}$	$\mathbf{P}_s^T \mathbf{s}_{t+k t}$	$\Omega_\psi \langle \psi_{t+k} \phi_t^T \rangle \Sigma_\phi^{-1} \phi_t + \mathcal{O}(T^{-1/2})$
$\mathbf{x}_{t+k t}$	$\Lambda_\psi^{-1/2} \mathbf{P}_\psi^T \Psi_{t+k t}$	$\Omega_x \langle \mathbf{x}_{t+k} \phi_t^T \rangle \Sigma_\phi^{-1} \phi_t + \mathcal{O}(T^{-1/2}) + \mathcal{O}(\sigma_x)$
$\mathbf{A}$	$\mathbf{P}_s$	$A \Omega_\psi^{-1} + \mathcal{O}(T^{-1/2})$
$\mathbf{B}$	$\langle \mathbf{x}_{t+2 t} \Psi_{t+1 t}^T \rangle_q \langle \Psi_{t+1 t} \Psi_{t+1 t}^T \rangle_q^{-1}$	$\Omega_x B \Omega_\psi^{-1} + \mathcal{O}(T^{-1/2}) + \mathcal{O}(\sigma_x)$
$\Psi$	$\langle \Psi_{t+2 t+2} \Psi_{t t}^T \rangle_q \langle \Psi_{t+1 t+1} \Psi_{t t}^T \rangle_q^{-1}$	$\Omega_\psi \Psi \Omega_\psi^{-1} + \mathcal{O}(T^{-1/2}) + \mathcal{O}(\sigma_\psi)$
$\Sigma_s$	$\langle \mathbf{s}_t \mathbf{s}_t^T \rangle_q$	$\Sigma_s + \mathcal{O}(T^{-1/2})$
$\Sigma_\psi$	$\frac{1}{2} (\Psi^{-1} \langle \Psi_{t+1 t+1} \Psi_{t t}^T \rangle_q$ $+ \langle \Psi_{t t} \Psi_{t+1 t+1}^T \rangle_q \Psi^{-T})$	$\Omega_\psi \Sigma_\psi \Omega_\psi^T + \mathcal{O}(T^{-1/2}) + \mathcal{O}(\sigma_\psi)$
$\Sigma_x$	$I$	$\Sigma_x \equiv I$
$\Sigma_\omega$	$\Sigma_s - \mathbf{A} \Sigma_\psi \mathbf{A}^T$	$\Sigma_\omega + \mathcal{O}(T^{-1/2}) + \mathcal{O}(\sigma_\psi)$
$\Sigma_z$	$\Sigma_x - \mathbf{B} \Sigma_\psi \mathbf{B}^T$	$\Omega_x \Sigma_z \Omega_x^T + \mathcal{O}(T^{-1/2}) + \mathcal{O}(\sigma_x)$
$\mathbf{N}_\psi$	$\underset{N_u}{\operatorname{argmin}} \mathcal{L}$	Converge to $N_\psi$ when $T > T_\psi^c$
$\mathbf{N}_x$	Largest spectrum gap of $\Sigma_\psi$	Converge to $N_x$ when $T > T_x^c$ and $\sigma_x < \sigma_x^c$

$\mathbf{P}_s$  and  $\mathbf{P}_\psi$  are sets of major eigenvectors of  $\Sigma_s$  and  $\Sigma_\psi$ , respectively; full-rank square matrix

$\Omega_\psi$  and orthogonal matrix  $\Omega_x$  are ambiguity factors;  $\sigma_x = \sqrt{(\overline{\rho^2} - \overline{\rho'^2}) \cdot N_x / N_\psi + \overline{\rho'''}^2 / N_x}$

and  $\sigma_\psi = \sqrt{(\overline{\rho^2} - \overline{\rho'^2}) / N_\psi}$  are linearization errors, where  $\sigma_x = \sigma_\psi = 0$  for any linear system;

$T_x^c, T_\psi^c < \infty$  are finite large constants and  $\sigma_x^c > 0$  is a small positive constant.

## Supplementary Information

### Dimensionality reduction to maximize prediction generalization capability

Takuya Isomura, Taro Toyoizumi

### Supplementary Movie legends

**Movie S1.** PredPCA of 90° rotated images, where the right-hand-side images are the predictions of the corresponding true images on the left-hand side. See **Fig. 3** legend and Method G for the detail.

**Movie S2.** PredPCA of 90° rotated images in the presence of an artificially added large observation noise. See **Fig. 3** legend and Method G for the detail.

**Movie S3.** PredPCA of natural scene movies. See **Fig. 4** legend and Method G for the detail.

### Supplementary Methods

#### S1. Generalization error for computing estimators

Suppose vectors  $\xi_t^l$  and  $\eta_t^l$  with  $l = 1, \dots, l_{max}$  as sequences of discrete time  $t$  with zero mean and consider the estimator of their outer product  $\theta^l \equiv \langle \xi_t^l \eta_t^{lT} \rangle_q$  calculated based on the

empirical distribution  $q$ . The estimator is decomposed into its true value  $\theta^l \equiv \langle \xi_t^l \eta_t^{lT} \rangle$  and the generalization error  $\delta\theta^l \equiv \boldsymbol{\theta}^l - \theta^l$ . Then, the expectation of the square of  $\delta\theta_{ij}^l$  is taken over an ensemble of different empirical distributions, which is denoted as  $E_{\{q\}}[\delta\theta_{ij}^l{}^2]$ . Under the assumption that  $(\xi_{ti}^l \eta_{tj}^l - \theta_{ij}^l)$  is independent in time, it is solved as

$$\begin{aligned} E_{\{q\}}[\delta\theta_{ij}^l{}^2] &= \text{plim}_{M \rightarrow \infty} \frac{1}{M} \sum_{m=1}^M \left( \frac{1}{T} \sum_{t=1}^T (\xi_{ti}^{l,m} \eta_{tj}^{l,m} - \theta_{ij}^l) \right)^2 = \frac{1}{T^2} \sum_{t=1}^T \langle (\xi_{ti}^l \eta_{tj}^l - \theta_{ij}^l)^2 \rangle \\ &= \frac{\langle (\xi_{ti}^l)^2 (\eta_{tj}^l)^2 \rangle - (\theta_{ij}^l)^2}{T} = \mathcal{O}(T^{-1}), \end{aligned} \quad (27)$$

where  $\xi_{ti}^{l,m}$  and  $\eta_{tj}^{l,m}$  indicates variables that are sampled from the  $m$ -th empirical distribution.

Here, the expectation  $E_{\{q\}}[\cdot]$  is computed by taking the average of the squared errors over  $M$

different empirical distributions and by diverging  $M$  to infinity (see Supplementary Method S2 for

the detail about this treatment). Hence, we obtain  $\delta\theta^l = \mathcal{O}(T^{-1/2})$  and thus  $\boldsymbol{\theta}^l = \theta^l +$

$\mathcal{O}(T^{-1/2})$  as the leading order.

Then, we define the estimator  $\boldsymbol{\theta}$  as the product of  $\boldsymbol{\theta}^1, \dots, \boldsymbol{\theta}^{l_{\max}}$ ,  $\boldsymbol{\theta} \equiv \prod_{l=1}^{l_{\max}} (\boldsymbol{\theta}^l)^{\alpha_l}$ , where

$(\boldsymbol{\theta}^l)^{\alpha_l}$  indicates either  $\boldsymbol{\theta}^l$  for  $\alpha_l = 1$  or the pseudo inverse of  $\boldsymbol{\theta}^l$ ,  $\boldsymbol{\theta}^{l+}$ , for  $\alpha_l = -1$ . Since each

$(\boldsymbol{\theta}^l)^{\alpha_l}$  becomes either  $\boldsymbol{\theta}^l = \theta^l + \delta\theta^l = \theta^l + \mathcal{O}(T^{-1/2})$  or  $\boldsymbol{\theta}^{l+} = \theta^{l+} - \theta^{l+} \delta\theta^l \theta^{l+} = \theta^{l+} +$

$\mathcal{O}(T^{-1/2})$ , as long as  $l_{\max}$  is a finite number, their product still has the  $T^{-1/2}$ -order

generalization error term. Therefore, we obtain

$$\boldsymbol{\theta} = \prod_{l=1}^{l_{\max}} \left( (\theta^l)^{\alpha_l} + \mathcal{O}(T^{-\frac{1}{2}}) \right) = \prod_{l=1}^{l_{\max}} (\theta^l)^{\alpha_l} + \underbrace{\mathcal{O}(T^{-\frac{1}{2}}) + \dots + \mathcal{O}(T^{-\frac{1}{2}})}_{l_{\max}} = \theta + \mathcal{O}(T^{-\frac{1}{2}}) \quad (28)$$

as the leading order.

## S2. Derivation of test prediction error expectation

Here, we calculate the expectation of the test prediction error. As described below, this is computed by taking the average of the generalization errors over an infinitely large number of different empirical distributions. A learner predicts the future input using the maximum likelihood estimator  $\mathbf{s}_{t+k|t} = \mathbf{Q}_k \phi_t$  and the set of the major eigenvectors of  $\Sigma_s = \frac{1}{K_f} \sum_{k=1}^{K_f} \langle \mathbf{s}_{t+k|t} \mathbf{s}_{t+k|t}^T \rangle_q$ ,  $\mathbf{P}_s$ , calculated based on the empirical distribution  $q$ . As the outer products are decomposed as  $\langle s_{t+k} \phi_t^T \rangle_q = \langle s_{t+k} \phi_t^T \rangle + \delta \langle s_{t+k} \phi_t^T \rangle_q$  and  $\langle \phi_t \phi_t^T \rangle_q^{-1} = \Sigma_\phi^{-1} - \Sigma_\phi^{-1} \delta \langle \phi_t \phi_t^T \rangle_q \Sigma_\phi^{-1} + \mathcal{O}(\delta \langle \phi_t \phi_t^T \rangle_q^2)$ , the estimator of the optimal mapping  $\mathbf{Q}_k = \langle s_{t+k} \phi_t^T \rangle_q \langle \phi_t \phi_t^T \rangle_q^{-1}$  becomes

$$\begin{aligned}
\mathbf{Q}_k &= (\langle s_{t+k} \phi_t^T \rangle + \delta \langle s_{t+k} \phi_t^T \rangle_q) (\Sigma_\phi^{-1} - \Sigma_\phi^{-1} \delta \langle \phi_t \phi_t^T \rangle_q \Sigma_\phi^{-1}) \\
&= \langle s_{t+k} \phi_t^T \rangle \Sigma_\phi^{-1} + \delta \langle s_{t+k} \phi_t^T \rangle_q \Sigma_\phi^{-1} - \langle s_{t+k} \phi_t^T \rangle \Sigma_\phi^{-1} \delta \langle \phi_t \phi_t^T \rangle_q \Sigma_\phi^{-1} \\
&= \underbrace{\langle s_{t+k} \phi_t^T \rangle \Sigma_\phi^{-1}}_{Q_k} + \underbrace{\delta \langle (s_{t+k} - Q_k \phi_t) \phi_t^T \rangle_q \Sigma_\phi^{-1}}_{\delta Q_k}
\end{aligned} \tag{29}$$

as the leading generalization error order, where  $Q_k \equiv \langle s_{t+k} \phi_t^T \rangle \Sigma_\phi^{-1}$  is the true optimal mapping and  $\delta Q_k = \delta \langle (s_{t+k} - Q_k \phi_t) \phi_t^T \rangle_q \Sigma_\phi^{-1}$  is the generalization error associated with the empirical distribution  $q$ . The squared average of the prediction error  $\varepsilon_{t+k|t}[q] \equiv s_{t+k} - \mathbf{P}_s \mathbf{P}_s^T \mathbf{Q}_k \phi_t$  over the true distribution provides the test prediction error, which is computed as

$$\left\langle |\varepsilon_{t+k|t}[q]|^2 \right\rangle = \text{tr}[\Sigma_s - \mathbf{P}_s \mathbf{P}_s^T \mathbf{Q}_k \langle \phi_t s_{t+k}^T \rangle - \langle s_{t+k} \phi_t^T \rangle \mathbf{Q}_k^T \mathbf{P}_s \mathbf{P}_s^T + \mathbf{P}_s \mathbf{P}_s^T \mathbf{Q}_k \Sigma_\phi \mathbf{Q}_k^T]$$

$$\begin{aligned}
&= \text{tr} \left[ \Sigma_s - \mathbf{P}_s \mathbf{P}_s^T \left( (Q_k + \delta Q_k) \Sigma_\phi Q_k^T + Q_k \Sigma_\phi (Q_k + \delta Q_k)^T - (Q_k + \delta Q_k) \Sigma_\phi (Q_k + \delta Q_k)^T \right) \right] \\
&= \text{tr} \left[ \Sigma_s - \mathbf{P}_s \mathbf{P}_s^T (Q_k \Sigma_\phi Q_k^T - \delta Q_k \Sigma_\phi \delta Q_k^T) \right] \\
&= \text{tr} \left[ \Sigma_s - \mathbf{P}_s \mathbf{P}_s^T Q_k \Sigma_\phi Q_k^T + P_s P_s^T \delta Q_k \Sigma_\phi \delta Q_k^T \right] + \mathcal{O} \left( T^{-\frac{3}{2}} \right) \tag{30}
\end{aligned}$$

as the leading generalization error order. Here, the generalization errors  $\delta Q_k$  and  $\delta P_s \equiv \mathbf{P}_s - P_s$  are in the  $T^{-1/2}$  order, so that the third term in the last equality is in the  $T^{-1}$  order.

Next, we compute the expectation of the test prediction error (Equation (17)). Here, we introduce the expectation over different empirical distributions, denoted as  $\mathbb{E}_{\{q\}}[\cdot]$ . The test prediction error expectation (Equation (18)) is computed as

$$\begin{aligned}
\mathcal{L} &= \mathbb{E}_{\{q\}} \left[ \frac{1}{2} \sum_{k=1}^{K_f} \left\langle |\varepsilon_{t+k|t}[q]|^2 \right\rangle \right] \\
&= \frac{1}{2} \sum_{k=1}^{K_f} \text{tr} \left[ \Sigma_s - \mathbb{E}_{\{q\}} [\mathbf{P}_s \mathbf{P}_s^T Q_k \Sigma_\phi Q_k^T] + P_s P_s^T \mathbb{E}_{\{q\}} [\delta Q_k \Sigma_\phi \delta Q_k^T] \right] + \mathcal{O} \left( T^{-\frac{3}{2}} \right) \\
&= \frac{K_f}{2} \text{tr}[\Sigma_s] - \frac{K_f}{2} \text{tr} \left[ \mathbb{E}_{\{q\}} [\mathbf{P}_s^T \Sigma_s \mathbf{P}_s] \right] + \frac{1}{2} \sum_{k=1}^{K_f} \text{tr} \left[ P_s^T \mathbb{E}_{\{q\}} [\delta Q_k \Sigma_\phi \delta Q_k^T] P_s \right] + \mathcal{O} \left( T^{-\frac{3}{2}} \right). \tag{31}
\end{aligned}$$

Below, we compute the expectation by regarding it as the average over an infinitely large number of different empirical distributions. In other words, for any estimator  $\boldsymbol{\theta} \equiv \langle \zeta_t \rangle_q$  that comprises an arbitrary function  $\zeta_t$  of random variables sampled from  $q$ , we suppose  $\mathbb{E}_{\{q\}}[\text{func}(\boldsymbol{\theta})] = \text{plim}_{M \rightarrow \infty} \frac{1}{M} \sum_{m=1}^M \text{func}(\boldsymbol{\theta}^m)$ , where  $\boldsymbol{\theta}^m \equiv \langle \zeta_t^m \rangle_{q_m}$  indicates the estimator based on the  $m$ -th empirical distribution  $q_m$ . The expectation of  $\boldsymbol{\theta}$  over an ensemble of  $q$  converges to the estimator computed based on the true distribution; i.e.,  $\mathbb{E}_{\{q\}}[\boldsymbol{\theta}] = \text{plim}_{M \rightarrow \infty} \frac{1}{MT} \sum_{m=1}^M \sum_{t=1}^T \zeta_t^m =$

$\langle \zeta_t \rangle = \theta$ . As  $\boldsymbol{\theta} = \theta + \delta\theta$ , the expectation of the generalization error converges to zero for any

estimator,  $E_{\{q\}}[\delta\theta] = O$ . Meanwhile, the expectation of the square of  $\boldsymbol{\theta}$  becomes  $E_{\{q\}}[\boldsymbol{\theta}\boldsymbol{\theta}^T] =$

$\theta\theta^T + E_{\{q\}}[\delta\theta\delta\theta^T]$ . Here,  $E_{\{q\}}[\delta\theta\delta\theta^T] = \text{plim}_{M \rightarrow \infty} \frac{1}{M} \sum_{m=1}^M \left( \frac{1}{T} \sum_{t=1}^T (\zeta_t^m - \theta) \right) \left( \frac{1}{T} \sum_{t=1}^T (\zeta_t^m - \theta) \right)^T$  is

a non-zero symmetric matrix. This is analytically solvable by assuming that the deviation  $(\zeta_t - \theta)$

is independent in time (i.e.,  $\langle (\zeta_t - \theta)(\zeta_{t'} - \theta)^T \rangle = O$  for  $t \neq t'$ ), which is given as

$$E_{\{q\}}[\delta\theta\delta\theta^T] = \text{plim}_{M \rightarrow \infty} \frac{1}{MT^2} \sum_{m=1}^M \sum_{t=1}^T (\zeta_t^m - \theta)(\zeta_t^m - \theta)^T = \frac{1}{T} \langle (\zeta_t - \theta)(\zeta_t - \theta)^T \rangle = \frac{1}{T} \langle \zeta_t \zeta_t^T \rangle - \theta\theta^T.$$

In particular, when we suppose that  $(s_{t+k} - Q_k \phi_t) \phi_t^T$  is independent in time and  $(s_{t+k} - Q_k \phi_t)$

is perpendicular to  $\phi_t$ , we find

$$\begin{aligned} E_{\{q\}}[\delta Q_k \Sigma_\phi^{-1} \delta Q_k^T] &= E_{\{q\}}[\delta \langle (s_{t+k} - Q_k \phi_t) \phi_t^T \rangle_q \Sigma_\phi^{-1} \delta \langle (s_{t+k} - Q_k \phi_t) \phi_t^T \rangle_q^T] \\ &= \frac{1}{T} \langle (s_{t+k} - Q_k \phi_t) \phi_t^T \Sigma_\phi^{-1} \phi_t (s_{t+k} - Q_k \phi_t)^T \rangle \\ &= \frac{1}{T} \langle (s_{t+k} - Q_k \phi_t) \langle \phi_t^T \Sigma_\phi^{-1} \phi_t \rangle (s_{t+k} - Q_k \phi_t)^T \rangle \\ &= \frac{N_\phi}{T} \langle (s_{t+k} - Q_k \phi_t) (s_{t+k} - Q_k \phi_t)^T \rangle \\ &= \frac{N_\phi}{T} (\Sigma_s - Q_k \Sigma_\phi Q_k^T). \end{aligned} \tag{32}$$

Thus, we obtain the analytical expression of the third term of Equation (31):

$$\sum_{k=1}^{K_f} \text{tr}[P_s^T E_{\{q\}}[\delta Q_k \Sigma_\phi^{-1} \delta Q_k^T] P_s] = \frac{K_f N_\phi}{T} \text{tr}[P_s^T (\Sigma_s - \Sigma_s) P_s]. \tag{33}$$

Finally, we show that the generalization error of the second term of Equation (31),

$\text{tr}[E_{\{q\}}[\mathbf{P}_s^T \Sigma_s \mathbf{P}_s]]$ , is negligible compared with the other generalization error term and thus it can

be approximated as  $\text{tr}[P_s^T \Sigma_s P_s]$  as the leading generalization error order. As  $\Sigma_s = \Sigma_s + \delta \Sigma_s$  and



$\mathbf{P}_s = P_s + \delta P_s$ ,  $\text{tr}[\mathbf{P}_s^T \Sigma_s \mathbf{P}_s]$  becomes

$$\begin{aligned} \text{tr}[\mathbf{P}_s^T \Sigma_s \mathbf{P}_s] &= \text{tr}[\mathbf{P}_s^T \Sigma_s \mathbf{P}_s] - \text{tr}[(P_s + \delta P_s)^T \delta \Sigma_s (P_s + \delta P_s)] \\ &= \text{tr}[\Lambda_s] - \text{tr}[P_s^T \delta \Sigma_s P_s + 2P_s^T \delta \Sigma_s \delta P_s] + \mathcal{O}\left(T^{-\frac{3}{2}}\right). \end{aligned} \quad (34)$$

Note that  $\delta P_s$  and  $\delta \Sigma_s$  are in the  $T^{-1/2}$  order and  $\delta \Sigma_s$  is a symmetric matrix. Thus, from

$\mathbb{E}_{\{q\}}[\Lambda_s] = \Lambda_s$  and  $\mathbb{E}_{\{q\}}[\delta \Sigma_s] = O$ , the expectation over an ensemble of  $q$  is given as

$$\text{tr}[\mathbb{E}_{\{q\}}[\mathbf{P}_s^T \Sigma_s \mathbf{P}_s]] = \mathbb{E}_{\{q\}}[\text{tr}[\mathbf{P}_s^T \Sigma_s \mathbf{P}_s]] = \text{tr}[\Lambda_s] - 2\mathbb{E}_{\{q\}}[\text{tr}[P_s^T \delta \Sigma_s \delta P_s]] + \mathcal{O}\left(T^{-\frac{3}{2}}\right). \quad (35)$$

The second term in the right-hand side can be rewritten as  $2 \sum_{i=1}^{N_u} \mathbb{E}_{\{q\}}[P_i^T \delta \Sigma_s \delta P_i]$  using the  $i$ -th eigenvector  $P_i \in \mathbb{R}^{N_s}$  of  $\Sigma_s$  and its generalization error  $\delta P_i \in \mathbb{R}^{N_s}$ . Here,  $\delta P_i$  is given as

$$\delta P_i = \sum_{j \neq i} \frac{P_j^T \delta \Sigma_s P_i}{\Lambda_i - \Lambda_j} P_j, \quad (36)$$

where  $\Lambda_i \in \mathbb{R}$  is the  $i$ -th eigenvalue of  $\Sigma_s$  [58]. Hence, we obtain

$$\mathbb{E}_{\{q\}}[\text{tr}[P_s^T \delta \Sigma_s \delta P_s]] = \mathbb{E}_{\{q\}}\left[\sum_{j \neq i} \frac{P_i^T \delta \Sigma_s P_j P_j^T \delta \Sigma_s P_i}{\Lambda_i - \Lambda_j}\right] = \sum_{j \neq i} \frac{P_i^T \mathbb{E}_{\{q\}}[\delta \Sigma_s P_j P_j^T \delta \Sigma_s] P_i}{\Lambda_i - \Lambda_j}. \quad (37)$$

By supposing that the deviation  $(\mathbf{s}_{t+k|t} \mathbf{s}_{t+k|t}^T - \Sigma_s)$  is independent in time, when  $i \neq j$ , the expectation is computed as

$$\begin{aligned} P_i^T \mathbb{E}_{\{q\}}[\delta \Sigma_s P_j P_j^T \delta \Sigma_s] P_i &= \frac{1}{T} P_i^T \langle (\mathbf{s}_{t+k|t} \mathbf{s}_{t+k|t}^T - \Sigma_s) P_j P_j^T (\mathbf{s}_{t+k|t} \mathbf{s}_{t+k|t}^T - \Sigma_s) \rangle P_i \\ &= \frac{1}{T} P_i^T \langle (\mathbf{s}_{t+k|t} \mathbf{s}_{t+k|t}^T P_j P_j^T \mathbf{s}_{t+k|t} \mathbf{s}_{t+k|t}^T) - \Sigma_s P_j P_j^T \Sigma_s \rangle P_i \\ &= \frac{1}{T} \langle (P_i^T \mathbf{s}_{t+k|t})^2 (P_j^T \mathbf{s}_{t+k|t})^2 \rangle \end{aligned}$$

$$\approx \frac{1}{T} \left\langle (P_i^T \mathbf{s}_{t+k|t})^2 \right\rangle \left\langle (P_j^T \mathbf{s}_{t+k|t})^2 \right\rangle = \frac{\Lambda_i \Lambda_j}{T}. \quad (38)$$

The approximation in the last line holds because the  $i$ -th eigenmode is almost independent of the  $j$ -th eigenmode. Thus, we obtain

$$\mathbb{E}_{\{q\}}[\text{tr}[P_s^T \delta \Sigma_s \delta P_s]] = \frac{1}{T} \sum_{i=1}^{N_u} \sum_{j \neq i} \frac{\Lambda_i \Lambda_j}{\Lambda_i - \Lambda_j} = \frac{1}{T} \sum_{i=1}^{N_u} \sum_{N_u+1 \leq j \leq N_\psi} \frac{\Lambda_i \Lambda_j}{\Lambda_i - \Lambda_j}. \quad (39)$$

Here,  $\sum_{i=1}^{N_u} \sum_{1 \leq j \leq N_u, j \neq i} \Lambda_i \Lambda_j / (\Lambda_i - \Lambda_j) = 0$  holds because of the symmetricity of indices  $i$  and  $j$ , and  $\Lambda_j = 0$  holds for  $j > N_\psi$ . Thus, the range of the sum is between  $N_u + 1 \leq j \leq N_\psi$  in the last equality. The expectation is bounded as

$$0 \leq \mathbb{E}_{\{q\}}[\text{tr}[P_s^T \delta \Sigma_s \delta P_s]] \leq \frac{N_u \sum_{N_u+1 \leq j \leq N_\psi} \Lambda_j}{(1-\kappa)T} \quad (40)$$

using a small positive constant  $\kappa$ . When  $N_u \geq N_\psi$ ,  $\mathbb{E}_{\{q\}}[\text{tr}[P_s^T \delta \Sigma_s \delta P_s]]$  is zero. When  $N_u < N_\psi$ , it is less than  $\frac{N_u \sum_{N_u+1 \leq j \leq N_\psi} \Lambda_j}{(1-\kappa)T}$ , which is much less than the other generalization error term (i.e., Equation (33)) because  $N_u \ll N_\phi$  and  $\sum_{N_u+1 \leq j \leq N_\psi} \Lambda_j \ll \text{tr}[P_s^T \Sigma_\omega P_s] < \text{tr}[P_s^T (\Sigma_s - \Sigma_s) P_s]$ . In other words,  $\sum_{N_u+1 \leq j \leq N_\psi} \Lambda_j$  means the sum of omitted minor eigenvalues of  $\Sigma_s$ , which is close to zero when  $N_u$  is close to  $N_\psi$ . Hence,  $\mathbb{E}_{\{q\}}[\text{tr}[P_s^T \delta \Sigma_s \delta P_s]]$  is negligible as the leading order and thus  $\text{tr}[\mathbb{E}_{\{q\}}[\mathbf{P}_s^T \Sigma_s \mathbf{P}_s]] \approx \text{tr}[\Lambda_s] + \mathcal{O}(T^{-3/2}) = \text{tr}[P_s^T \Sigma_s P_s] + \mathcal{O}(T^{-3/2})$  holds. Therefore, by substituting the above results into Equation (31), we obtain Equation (19).

### S3. Derivation of the order of the linearization error term

The order of the linearization error term  $\mathcal{O}(\sigma_\psi)$  is identified, by computing the variance of

$\langle \Delta \psi_{t+2|t+1} \psi_t^T \rangle \Sigma_\psi^{-1/2}$  averaged over all elements,  $\sigma_\psi^2 \equiv \frac{1}{N_\psi^2} \text{tr}[\langle \Delta \psi_{t+2|t+1} \psi_t^T \rangle \Sigma_\psi^{-1} \langle \psi_t \Delta \psi_{t+2|t+1}^T \rangle]$ .

Here,  $\frac{1}{N_\psi^2} \text{tr}[\langle \Delta \psi_{t+2|t+1} \psi_t^T \rangle \Sigma_\psi^{-1} \langle \psi_t \Delta \psi_{t+2|t+1}^T \rangle]$  is the variance of the maximum likelihood

estimator  $\langle \Delta \psi_{t+2|t+1} \psi_t^T \rangle \Sigma_\psi^{-1} \psi_t$ . From the asymptotic linearization theorem [33], the hidden basis

$\psi_t$  is decomposed into the linear mapping of  $x_t$  and the residual  $\eta_t$  that is perpendicular to  $x_t$ ,

given as  $\psi_t = P \Lambda^{1/2} x_t + \eta_t$  as the leading order. Here,  $P \in \mathbb{R}^{N_\psi \times N_x}$  and  $\Lambda \in \mathbb{R}^{N_x \times N_x}$  are the

major eigenvectors and eigenvalues of  $\Sigma_\psi$ , and  $\eta_t$  satisfies  $\langle \eta_t \rangle = 0$  and  $\langle \eta_t \eta_t^T \rangle = (\overline{\rho^2} -$

$\overline{\rho'^2}) CC^T$ . From Equation (9),  $\psi_{t+1} = P \Lambda^{1/2} B \psi_t + \eta_{t+1} + \mathcal{O}(z_t)$  holds. Since  $\Psi$  is the optimal

(maximum likelihood) linear mapping from  $\psi_t$  to  $\psi_{t+1}$ , the prediction using  $\Psi$  must be more

accurate than that using the lower-rank linear mapping  $P \Lambda^{1/2} B$ . This means that the variance (i.e.,

prediction error) of the predicted residual  $\langle \Delta \psi_{t+2|t+1} \psi_t^T \rangle \Sigma_\psi^{-1} \psi_t = (\langle \psi_{t+2} \psi_t^T \rangle \Sigma_\psi^{-1} - \Psi^2) \psi_t$  is

smaller than that of the predicted nonlinear components  $\langle \eta_{t+2} \psi_t^T \rangle \Sigma_\psi^{-1} \psi_t = (\langle \psi_{t+2} \psi_t^T \rangle \Sigma_\psi^{-1} -$

$P \Lambda^{1/2} B \Psi) \psi_t$ . Hence, we obtain  $\text{tr}[\langle \Delta \psi_{t+2|t+1} \psi_t^T \rangle \Sigma_\psi^{-1} \langle \psi_t \Delta \psi_{t+2|t+1}^T \rangle] \leq \text{tr}[\langle \eta_{t+2} \psi_t^T \rangle \Sigma_\psi^{-1} \langle \psi_t \eta_{t+2}^T \rangle]$ .

As the maximum likelihood estimator's variance must be smaller than the actual value's variance,

$\text{tr}[\langle \eta_{t+2} \psi_t^T \rangle \Sigma_\psi^{-1} \langle \psi_t \eta_{t+2}^T \rangle] \leq \text{tr}[\langle \eta_{t+2} \eta_{t+2}^T \rangle] = (\overline{\rho^2} - \overline{\rho'^2}) \text{tr}[CC^T] = \mathcal{O}\left(N_\psi (\overline{\rho^2} - \overline{\rho'^2})\right)$  holds.

Therefore, we find  $\sigma_\psi = \sqrt{(\overline{\rho^2} - \overline{\rho'^2}) / N_\psi}$  as the order.

The orders of the linearization error term in Equations (22) and (23) are computed as follows, by

using  $\langle \Delta \psi_{t+2|t+1} \psi_t^T \rangle \Sigma_\psi^{-1/2} = \mathcal{O}(\sigma_\psi)$ . As  $\text{tr}[\langle \Delta \psi_{t+2|t+1} \psi_t^T \rangle \Sigma_\psi^{-2} \langle \psi_t \Delta \psi_{t+2|t+1}^T \rangle] =$

$\text{tr}\left[\left(\langle \Delta \psi_{t+2|t+1} \psi_t^T \rangle \Sigma_\psi^{-1/2}\right) \Sigma_\psi^{-1} \left(\langle \Delta \psi_{t+2|t+1} \psi_t^T \rangle \Sigma_\psi^{-1/2}\right)^T\right] \approx N_\psi \sigma_\psi^2 \text{tr}[\Sigma_\psi^{-1}] = \mathcal{O}(N_\psi^2 \sigma_\psi^2),$

$\langle \Delta \psi_{t+2|t+1} \psi_t^T \rangle \Sigma_\psi^{-1} = \mathcal{O}(\sigma_\psi)$  holds as the order. Thus, the order of the linearization error term in

Equation (22) is  $\mathcal{O}(\sigma_\psi)$ . Moreover, we have

$$\begin{aligned}
\Psi^{-1} \langle \Psi_{t+1|t+1} \Psi_{t|t}^T \rangle_q &= \Omega_\psi (\Psi^{-1} - \Psi^{-1} \langle \Delta \psi_{t+2|t+1} \psi_t^T \rangle_{\Sigma_\psi^{-1}} \Psi^{-2}) \Omega_\psi^{-1} \cdot \Omega_\psi \Psi \Sigma_\psi \Omega_\psi^T + \mathcal{O}(T^{-\frac{1}{2}}) \\
&= \Omega_\psi \Sigma_\psi \Omega_\psi^T - \Omega_\psi \Psi^{-1} \langle \Delta \psi_{t+2|t+1} \psi_t^T \rangle_{\Sigma_\psi^{-1}} \Psi^{-1} \Sigma_\psi \Omega_\psi^T + \mathcal{O}(T^{-\frac{1}{2}}) \\
&\approx \Omega_\psi \Sigma_\psi \Omega_\psi^T - \Omega_\psi \Psi^{-1} \langle \Delta \psi_{t+2|t+1} \psi_t^T \rangle \Psi^T \Omega_\psi^T + \mathcal{O}(T^{-\frac{1}{2}}), \tag{41}
\end{aligned}$$

where  $\Sigma_\psi \approx \Psi \Sigma_\psi \Psi^T$  was used. Similarly, as  $\text{tr}[\langle \Delta \psi_{t+2|t+1} \psi_t^T \rangle \langle \psi_t \Delta \psi_{t+2|t+1}^T \rangle] =$

$$\text{tr} \left[ \left( \langle \Delta \psi_{t+2|t+1} \psi_t^T \rangle_{\Sigma_\psi^{-1/2}} \right) \Sigma_\psi \left( \langle \Delta \psi_{t+2|t+1} \psi_t^T \rangle_{\Sigma_\psi^{-1/2}} \right)^T \right] \approx N_\psi \sigma_\psi^2 \text{tr}[\Sigma_\psi] = \mathcal{O}(N_\psi^2 \sigma_\psi^2),$$

$\langle \Delta \psi_{t+2|t+1} \psi_t^T \rangle = \mathcal{O}(\sigma_\psi)$  holds as the order. Therefore, the order of the linearization error term in

Equation (23) is  $\mathcal{O}(\sigma_\psi)$ .

## References

58. Griffiths, D. J. *Introduction to quantum mechanics*. 2nd ed. (Pearson Prentice Hall, 2005).